Porous ferroelectric materials for energy technologies: current status and future perspectives

Mingyang Yan,^a Zhida Xiao,^a Jingjing Ye,^a Xi Yuan,^b Zihe Li,^c Chris Bowen,^c Yan Zhang^{a*} and Dou Zhang^{a*}

- ^a State Key Laboratory of Powder Metallurgy, Central South University, Changsha, Hunan 410083, China.
- b Gllege of Chemistry and Chemical Engineering, Central South University, Changsha,
 Hunan 410083, China.
- ^c Department of Mechanical Engineering, University of Bath, United Kingdom, Bath, BA27AY, UK

Corresponding Authors

* E-mail: yanzhangcsu@csu.edu.cn (Yan Zhang); dzhang@csu.edu.cn (Dou Zhang);

Abstract: Ferroelectric materials have attracted significant interest due to their wide potential in energy harvesting, sensing, storage and catalytic applications. For monolithic and dense ferroelectric materials, their performance figures of merit for energy harvesting and sensing are limited by their high relative permittivity, and their low surface area can limit piezo- or pyro-catalytic applications. As a result, the introduction of porosity into dense ferroelectric materials can enhance performance for a variety of piezoelectric and pyroelectric applications. In this review, the piezoelectric, pyroelectric, ferroelectric and mechanical properties of porous ferroelectrics are presented, and the fabrication processes to create porous ferroelectric materials are classified and discussed. Simulations of the poling process and resulting piezo- and pyro-electric properties are also described to understand the underlying science of these fascinating porous materials and develop new approaches towards materials design. Applications of porous ferroelectric materials in specific fields are then summarized. Finally, conclusions and future perspectives for porous ferroelectric materials are provided.

Key words: porous ferroelectric materials; piezoelectric; pyroelectric; sensors; energy harvesting

1. Introduction

With the rapid development of global industry, the economy and world population, the energy crisis and associated environmental pollution have become serious challenges for our society. The growth in the Internet of Things (IoT) has also led to an increase in the need for smart sensors to detect pressure, force, acceleration and heat, including piezo- and pyro-electric based sensors.

The need to provide power for the increasing number of distributed sensors has also led to growing interest in energy harvesting to reduce our reliance on electrical cables and batteries, and their maintenance. There are a wide range of energy sources in our living ambient environment, which includes wind, light, heat, and mechanical vibrations; these energies are often wasted if they are not efficiently utilized. Energy harvesting technologies, which are able to convert such energy sources into electricity, have attracted much attention in recent years. Among the variety of available energy harvesting technologies, piezoelectric and pyroelectric energy harvesting, which transfer mechanical vibrations and thermal fluctuations into electricity, have attracted significant interest due to their high power density, integration and low electromagnetic interference.

Ferroelectric materials are commonly used in the field of sensors, energy harvesting, actuators, and catalysis since they can exhibit the *piezoelectric* effect. ⁹ The piezoelectric effect was first discovered in 1880 by the Curie brothers. ¹⁰ As shown in Fig. 1, the *direct* piezoelectric effect relates to the conversion of a mechanical stress, or

strain, into an electric charge, or potential, due to a change in polarization, which makes it of interest for applications related to *sensors* that can detect pressure or accelerations and *energy harvesters* that aim to use the electrical charge to provide power for low power electronics. With regard to the *converse* piezoelectric effect, a mechanical strain or force is generated in response to an applied electric field due to an extension or contraction of the electrical dipole responsible for the polarization, which is of interest for actuators applications such as micro-positioners, high speed valves and loudspeakers.

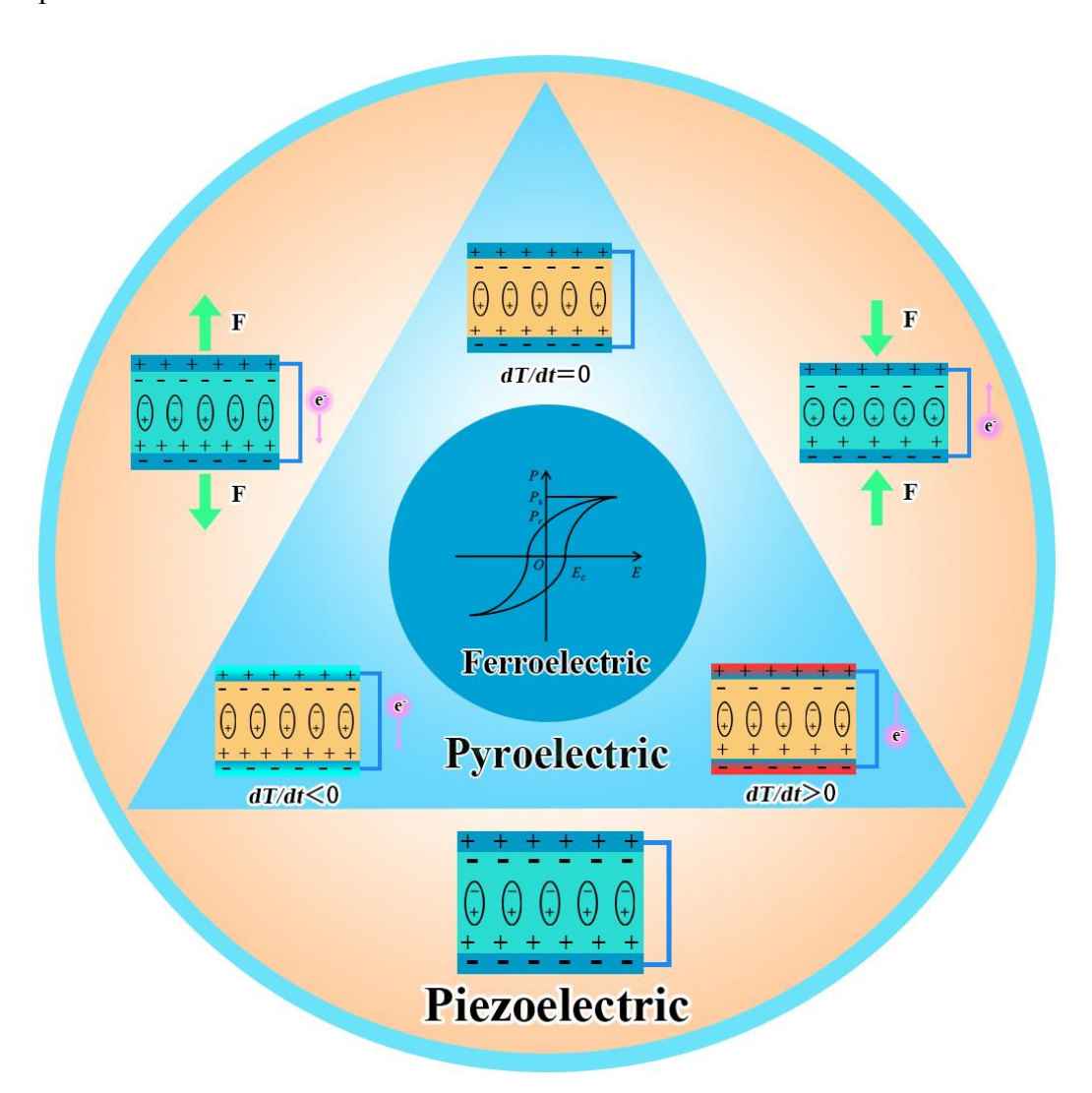


Fig. 1 Interrelationship between piezoelectric, pyroelectric and ferroelectric materials.

Pyroelectric materials are a sub-class of piezoelectric materials that are able to convert a change in temperature into electric charge as a result of a change in polarization with temperature. As a result, they can be utilized for thermal sensing, such as infrared/person detection and thermal imaging. Ferroelectric materials are a further sub-category of these materials, see Fig.1, which exhibit a spontaneous polarization that can be switched by an external electric field or mechanical stress giving rise to a typical hysteretic behavior between polarization and electric field. Therefore, all ferroelectric materials can be both piezoelectric and pyroelectric, since their polarization changes with mechanical stress (piezo-) and temperature (pyro-), respectively. The unique multi-functional properties of ferroelectric materials allow them to both sense and harvest energy from both mechanical vibrations and thermal fluctuations.

To assess the ability of ferroelectric materials for piezoelectric and pyroelectric energy harvesting and sensing applications, a variety of performance figures of merit have been developed. With regard to piezoelectric and pyroelectric sensing applications, the following parameters and figures of merit can be used to assess their performance.

$$g_{33} = \frac{d_{33}}{\varepsilon_{33}^T \varepsilon_0} \tag{1}$$

$$g_h = \frac{d_{33} + 2d_{31}}{\varepsilon_{33}^T \varepsilon_0} \tag{2}$$

$$F_V = \frac{p}{C_E \varepsilon_{33}^T \varepsilon_0} \tag{3}$$

Where d_{33} and d_{31} are the longitudinal and transverse piezoelectric charge coefficients, ε_{33}^T is the relative permittivity at constant stress, ε_0 is the permittivity of

free space, p is the pyroelectric coefficient, C_E is the volume specific heat capacity. The g_{33} parameter is the piezoelectric voltage coefficient and is a measure of the electric field, and therefore voltage, generated from a stress in the polarization direction. This parameter is of interest for sensing elements subjected to a uniaxial load in the polarization direction. The parameter g_h is the *hydrostatic* voltage coefficient and is a measure of the electric field per unit hydrostatic stress; this parameter is typically of interest for low frequency SONAR applications where the mechanical load is applied to all surfaces of the piezoelectric element. The F_V figure of merit is related to the voltage developed due to the pyroelectric effect in response to temperature change.

While the parameter for sensing above relate to the open circuit voltage developed in response to mechanical and thermal stimuli, for energy harvesting the energy generated is important and the piezo- and pyro-electric figures of merit can be defined by the following equations 3 46 :

$$FoM_{ij} = \frac{d_{ij}^2}{\varepsilon_0 \varepsilon_{33}^T} \tag{4}$$

$$F_E' = \frac{p^2}{\varepsilon_0 \varepsilon_{13}^T \times (C_E^2)} \tag{5}$$

where d_{ij} is the piezoelectric charge coefficient. The FoM_{ij} parameter is a piezoelectric energy harvesting figure of merit and is a measure of the energy density for a mechanical stress, and F'_E is a pyroelectric energy harvesting figure of merit and is a measure of the energy density for a given thermal input. It can be seen from the above equations that the harvested piezoelectric and pyroelectric energy density and sensing performance strongly depend on the piezoelectric charge coefficient, d_{ij} , the pyroelectric coefficient, p, the volume specific heat capacity, C_E and the relative

permittivity, ε_{33}^T . Therefore, a high d_{ij} and low ε_{33}^T are desirable for piezoelectric energy harvesting and piezo-sensing applications, while a high p, low ε_{33}^T and C_E are beneficial for pyroelectric energy harvesting and sensing applications. It is striking to see that all the figures of merit for sensing and harvesting are *inversely proportional* to the relative permittivity, ε_{33}^T , and a key factor to enhance the energy harvesting and sensing performance is to the reduce the relative permittivity of ferroelectric materials while also achieving a high piezo- and pyro-electric activity.

Ferroelectric materials are often commercially produced with high relative densities and low porosity levels in an effort to maximize their piezoelectric and pyroelectric properties, and limit mechanical and electrical stress concentrations due to the presence of defects, which can initiate fracture or dielectric breakdown.^{17,18} However, due to their ease of polarization, the relative permittivity of dense ferroelectric materials is typically high, which can limit the performance figures of merit described above; for example, the relative permittivity of dense barium titanate (BaTiQ) is $\varepsilon_{33}^T \sim 1400$ and for some lead zirconate titanate materials (PZT), $\varepsilon_{33}^T >$ 3000. While the existence of porosity is often considered as a defect, the introduction of porosity can act positively to significantly reduce the relative permittivity, and enhance the figures of merit for sensing and harvesting described above.¹⁹ ²² Therefore, in recent years, research has been conducted on porous ferroelectric materials to reduce the effective permittivity, while being able to maintain the piezo- and pyro-electric coefficients and mechanical or electrical strength. A variety of fabrication technique³ ²⁵ have been developed to obtain porous materials with high performance, such as the

burnt-out polymer spheres method and freeze casting, and the effect of porosity fraction, shape, and orientation on the properties of porous ferroelectric materials have been studied. Since the process of *poling* is crucial in achieving a high remnant polarization and developing a piezoelectric and pyroelectric response, both experimental and simulation studies have been conducted to understand how the poling process is influenced by the presence of porosity in ferroelectrics. A variety of porous structures have also been designed to optimize the piezoelectric and pyroelectric properties of porous ferroelectric materials. While the development of porous ferroelectric materials is continuing to grow, there continues to be a number of exciting scientific and engineering challenges for further develop and exploit porosity in ferroelectrics.

A small number of excellent reviews and book chapters exist that focus on porous ferroelectric materials, ^{8 30} which have primarily summarized the fabrication techniques of porous ferroelectric ceramics and their applications for energy harvesting applications and hydrophones for SONAR. Since the classification, characterization, simulation, and applications of porous ferroelectric materials for energy technologies have yet to be summarized, an intensive and comprehensive review on porous ferroelectric materials is timely. As a result, a comprehensive and systematic review is now provided to summarize the most recent developments of porous ferroelectric materials, and Fig. 2 presents a review outline. Firstly, the range of porous piezoelectric materials are presented. Secondly, the fabrication techniques of porous ferroelectric are summarized. Thirdly, the dielectric, ferroelectric, piezoelectric, pyroelectric, and

mechanical properties of porous ferroelectrics are systematically evaluated. The modelling, design and applications of porous ferroelectric materials are then discussed. Finally, the critical challenges and outlook are proposed to promote the development of high performance porous ferroelectric materials.

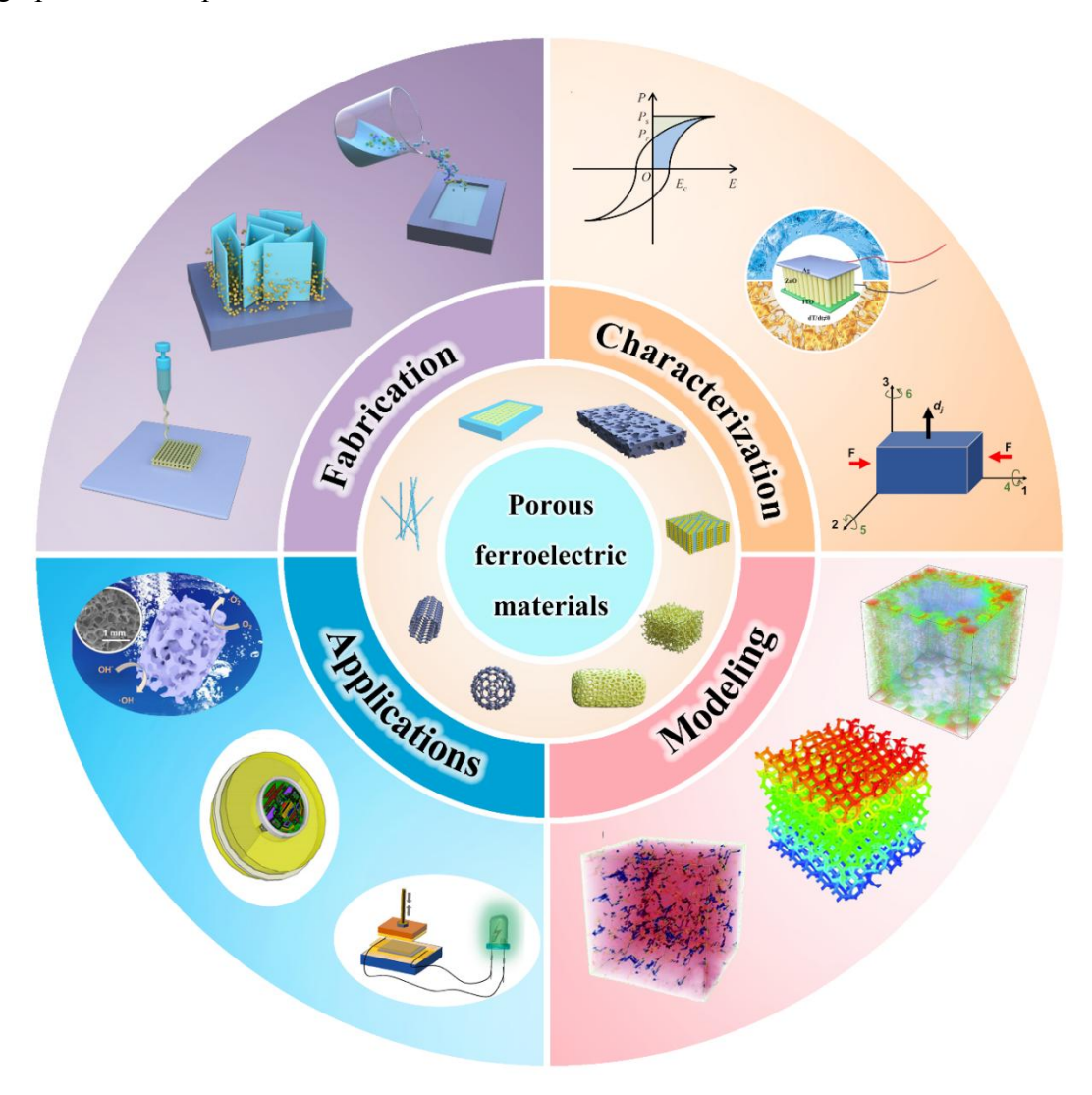


Fig. 2 Summary of porous ferroelectric materials, and their fabrication, characterization, simulation, and relevant applications.

2. Porous ferroelectric materials

Porous ferroelectric materials are attracting interest due to their potential benefits in energy harvesting, sensing, SONAR, and catalytic applications compared with dense

ferroelectric materials. Generally, current porous ferroelectric materials can be classified into four categories: (i) porous ceramics, (ii) porous polymers, (iii) porous composites, and (iv) porous thin-films and nanostructures.

2.1 Porous ferroelectric ceramics

Porous ferroelectric ceramics occupy an important position in porous ferroelectric materials since the majority of research to date has been performed on ceramic-based porous materials. Many ferroelectric ceramics exhibit a perovskite structure, which possess enhanced ferroelectric properties compared to other ceramic systems, ³ 1 such as bismuth-layer and tungsten bronze structure ferroelectrics. The most widely studied porous perovskite-structure ferroelectric is based on the lead zirconate titanate (Pb[Zr_xTi_x]O, PZT) family due to their excellent piezoelectric and ferroelectric properties.^{3 2 ,3 3} Research to date on porous ferroelectric ceramics has included PZT, lead magnesium niobate-lead zirconate titanate² (PMN-PZT), lead zirconate titanatelead cobalt niobate (PZT-PZN) and Nb-doped PZT^{3,4} Unfortunately, the toxicity of Pb can restrict its applications, since it is unfriendly to our living environment and human health, with growing legislation to reduce the use of lead in electronic applications and in electronic waste (e-waste). Therefore, a number of studies on porous lead-free ferroelectric ceramics have recently been developed.^{3,5,36} Among them, porous barium calcium zirconate titanate (BCZT) has attracted attention due to the high piezoelectric d_{33} charge coefficient of this material.³⁷ ³⁸

Porous ferroelectric ceramics can also be considered as a *composite*, since they are the combination of two phases, namely a ferroelectric ceramic matrix and a pore phase

that simply contains air. Newnham et al. developed an approach to describe the structure of piezoelectric composites using two numbers based on the connectivity and the interconnection of the individual phases.³⁹,⁴⁰ Porous ferroelectric ceramics can be classified into 3-0, 3-1, 3-3, and 2-2 types according to the connectivity of the pores and the piezoelectric ceramic, as shown in Fig. 3. The first number indicates the connectivity of the active piezoelectric phase while the second number indicates the connectivity of the passive pore phase.⁴ Porous ferroelectric ceramics with a 3-0 structure therefore consist of isolated pores in a continuous ferroelectric matrix and have the advantages of ease of preparation and potential to be made with a wide range of porosity². In 3-3 type porous ferroelectric ceramics both the ceramic matrix and pores are fully interconnected, and these porous materials usually possess better acoustic properties compared to the dense material, since the introduction of pores can reduce its acoustic impedance (Z), leading to improved coupling of waves between a piezoelectric generator, sensor, and the propagating media; for example air, water or biological tissue.⁴³ However, the mechanical performance of these two types of porous ferroelectric ceramics is often limited by the inhomogeneity of the structure. The 3-1 type materials (aligned pores in a continuous ceramic matrix) and 2-2 type materials (alternating 2-D layers of ceramic and pores) exhibit improved piezoelectric properties due to the orientation of piezoelectric phase in the poling direction, ⁴², ⁴⁴ for example, porous BCZT ceramic with 2-2 type structure possessed a higher remnant polarization compared to a 3-0 structure due to greater fraction of poled regions in ceramics.⁴⁵ Less research has been undertaken of 3-1 and 2-2 type porous structures, and it would be of interest to undertake more research in this area in an effort to improve level of polarization and facilitate the poling process.

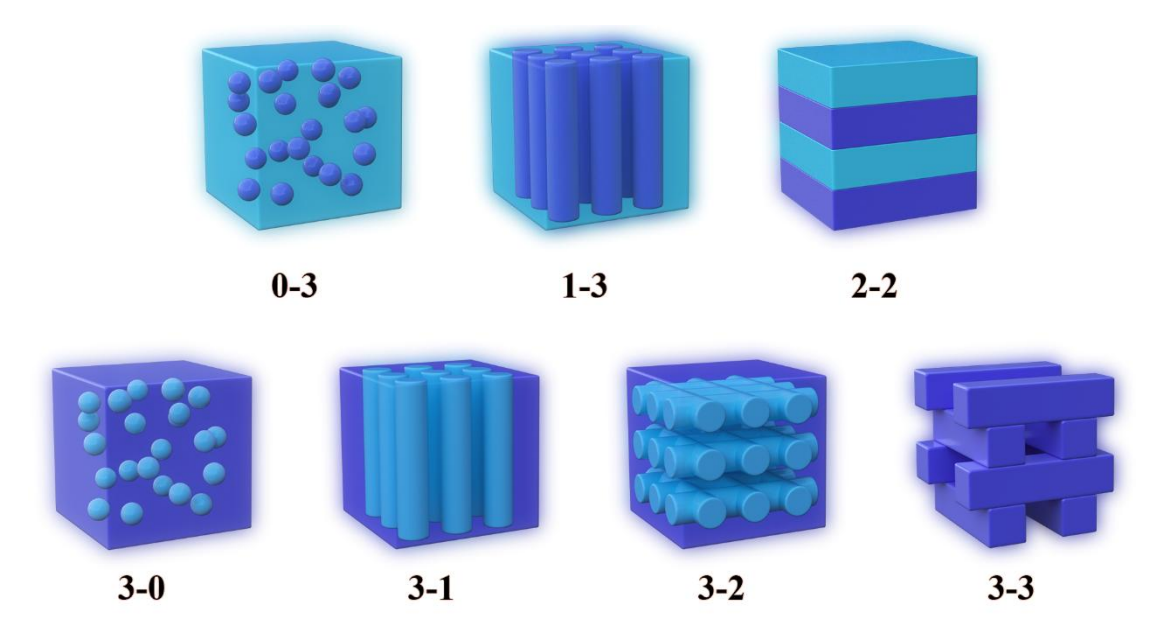


Fig. 3 Different types of connectivity of the two-phase ferroelectric composite.

2.2 Porous ferroelectric polymers

In recent years, porous ferroelectric polymers have attracted interest because of their lightweight nature, mechanical flexibility and biocompatibility for medical sensing and harvesting. Among the available ferroelectric polymers, the most popular is polyvinylidene difluoride (PVDF), and its copolymers. The piezoelectricity of PVDF originates from the ferroelectric orientation of dipolar crystals and there are five crystalline phases in PVDF and its copolymers, namely α , β , γ , δ and ϵ . The α -phase is the most common phase, where the dipoles are arranged in reverse parallel, which leads to no significant piezoelectricity. However, the β -phase and γ -phase are polar crystalline phases, since the dipoles in the β -phase and γ -phase are arranged in parallel; therefore, the piezoelectric properties of PVDF is primarily attributed to these two phases. As a result, approaches to increase the content of β -phase and γ -phase in

porous PVDF a top of intense research.

In general, porous ferroelectric polymers created using PVDF are based on two kinds of structures, a porous *surface* structure whereby pores are located only on the polymer surface and a *bulk* porous structure, where pores are distributed throughout the whole material. These two kinds of structures are produced by a template-assisted method and phase separation method, respectively. Compared with dense ferroelectric polymers, porous structures have enhanced sensitivity to mechanical vibrations due to a local increase in stress intensity and the enlargement electrode area for charge collecting, making porous ferroelectric polymers promising candidates for PVDF-based piezoelectric nano-devices.

2.3 Porous ceramic-based ferroelectric composites

Ferroelectric composites are typically formed using two phases, an electro-active ferroelectric phase and an inert polymer phase. While a porous ferroelectric ceramic that consists of a ceramic matrix and pores (air) can be considered as a piezoelectric composite, in this review a porous ceramic-based ferroelectric *composite* refers to the combination of a porous ferroelectric ceramic with a polymer, where the pores are infiltrated with a polymer phase to provide an additional functionality, such as mechanical flexibility or toughness. Epoxy resin and polydimethylsiloxane (PDMS) are often selected as a second phase polymer to infill the pores of a porous ferroelectric ceramics; these materials are selected due to their low viscosity and attractive flow properties to impregnate pores prior to curing. Since porous 3-0 based ferroelectric ceramics contain pores that are isolated, the impregnation of pores in difficult. However,

a polymer can more readily fill the open pores of 3-1, 3-3 and 2-2 type porous ferroelectric ceramics, due to the inter-connected pore structure. Research has been conducted on porous ceramic-based ferroelectric composites since they are less brittle, high toughness and more flexible compared to the initial porous ferroelectric ceramic, thereby providing new application areas such as flexural vibration energy harvesting and conformable sensors for wearable applications or complex geometries.

2.4 Porous thin-films and nanostructures

In addition to the above mentioned porous ferroelectric materials, porous ferroelectric thin-films and porous ferroelectric nano-structures are being developed. Ferroelectric thin films are a class of ferroelectric material, which are often based on ferroelectric oxides, such as Pb(Zr,Ti)Q (Ba,Sr)TiQ and BiFeQ .55 58 Fabrication methods for ferroelectric thin-films include radio-frequency (RF) sputtering, metalorganic chemical deposition, electron beam evaporation, pulsed laser deposition and the sol-gel method. The introduction of porosity into ferroelectric thin films can enhance the piezoelectric response, since the introduction of porosity can eliminate the clamping effects of the substrate and make the ferroelectric domain walls mobile.⁵⁵ For example, compared to dense ferroelectric films, porous films can exhibit an coefficient approximately three-times larger piezoelectric improved and electromechanical response; where the most commonly studied porous ferroelectric thin films are PZT-based thin films. Ferroelectric nanomaterials can be divided into three groups according to their dimension; these include (i) zero-dimensional nanomaterials, such as nanoparticles; (ii) one-dimensional nanomaterials, generally referred to as nanowires, nanotubes, and nanofibers; (ii) two-dimensional nanomaterials, such as nanosheets. Porous ferroelectric nanomaterials generally refer to one-dimensional and two-dimensional materials, for example, porous PbTiQ nanowires. Now that the range of porous ferroelectrics have been introduced, the range of methods to create the porous materials are now described.



Fig. 4 Core fabrication techniques for the manufacture of porous ferroelectric materials.

3. Fabrication techniques for porous ferroelectric materials

After several decades of research efforts, a variety of methods for the fabrication

of porous ferroelectric materials have been developed. The primary fabrication techniques are summarized in Fig. 3, including the burnt-out polymer spheres method (BURPS), the replica template method, gel casting, freeze casting and additive manufacturing. The corresponding morphologies of porous piezoelectric materials obtained by these methods are presented in Fig. 4 to help understand the fabrication techniques and the microstructures and geometries that can be formed.

3.1 Burnt-out polymer spheres (BURPS)

The burnt-out polymer spheres method is the most conventional and frequently used technique to fabricate porous ferroelectric ceramics. In this method, ferroelectric ceramic powders are mixed with polymer spheres or another low temperature material, and the ferroelectric ceramic green bodies are obtained via uni-axially pressing, isostatic pressing or tape casting methods. During the sintering process, the polymer spheres or additive are burnt out, thereby forming the pore structure during the volatilization process. The selection of the appropriate pore-forming agents is important, and it is essential that the pore-forming agents do not react with the ceramic matrix during the burn-out and sintering process. A number of pore-forming agents have been used to fabricate porous ferroelectric ceramics, which are often spherical in shape; these include polymers and organic materials such as polymethyl methacrylate (PMMA) spheres, polyethylene oxide (PEO), polyethylene (PE) beads, stearic acid (SA), polyvinyl chloride (PVC), dextrin, ellulose, ellulose, glucose, glucose, saccharose⁶⁷ polystyren^{§ 8}. In addition, non-spherical pore-forming agents have been used, such as polyethylene fiber and graphene.^{62,69} By selecting pore-forming agents with different

shapes, the morphology, pore size and pore structure of the porous ferroelectric ceramics can be tailored. The pore size of porous ceramics fabricated by this method typically ranges from 0.1 to 300 µm, depending on the geometry of pore-forming agents. In addition, it has been shown that the porosity can be controlled by adjusting the volume fraction of the volatile filler. The final pore volume fraction is not exactly the same as the initial volume fraction of the additive, since there is some shrinkage of the ceramic during the high-temperature sintering process. Nevertheless, a clear correlation between the volume fraction of polymer spheres and the porosity level was shown by Wang *et al.*, where the final porosity levels were lower than the initial volume fraction of the pore-forming agents, but increasing the fraction of pore-forming agents led to higher levels of porosity.

Different pore-forming agents have also been investigated, where Zeng *et al.* prepared porous PZT ferroelectric ceramics via burnt-out polymer spheres method using PMMA with spherical or irregular shapes as the pore-forming agent. As shown in Fig. 5a, it was observed that the pore shape and size were determined by the shape and sizes of pore formers. Zhang *et al.* used both PMMA and stearic acid to fabricate porous ferroelectric ceramics. The PMMA-derived pores were approximately spherical, while the stearic acid resulted pores were mostly irregular, and many pore channels and voids can be observed. For the two kinds of pore-forming agent examined, when the volume fraction was greater than 30%, the pores became interconnected and, as the volume fraction increased from 10% to 50%, the microstructure changed from a 3-0 type structure with isolated pores to a 3-3 type structure with interconnected,

indicating a strong correlation between the degree of pore interconnectivity and the volume fraction of the pore forming agent.

While the burnt-out polymer spheres method has the advantages of easy fabrication and low cost, there are some disadvantages. For example, polymer spheres cannot be easily mixed uniformly with ferroelectric ceramic powders. As a result, the pores that are formed are often distributed randomly throughout the ceramic structure and can be agglomerated. One disadvantage of the burnt-out polymer spheres method is the development of cracks in the ceramic matrix, which can be formed during the volatilization of the additive during the burn out process or the initial pressing process. When the volume fraction of polymer spheres are high, they can began to agglomerate, to form highly interconnected pores and develop cracks in the porous ferroelectric ceramic.⁷³ Praveenkumar *et al.* observed cracks in a porous ceramic, where the cracks were orientated perpendicular to the pressing direction when the volume fraction of PMMA was 50%.⁷⁴, which led to poor mechanical properties; the formation to such cracks was possibly related to the recovery of elastic strain by the polymer filler once the uni-axial pressure was removed. The maximum porosity fraction obtained by this method is limited to 60-70% due to a reduction in mechanical strength above this point; for example the loss of such a large volume fraction of polymer during the burn out stage can lead to loss of mechanical integrity of the ceramic prior to sintering ⁷⁵ As a result, porous ferroelectric ceramics with high porosity fractions (>60%) cannot be readily fabricated by this method. Moreover, the pores obtained by this method were always randomly distributed, and pore alignment cannot be efficiently controlled in an

attempt to improve the poling process.

3.2 Gel casting

Gel casting was initially developed to fabricate dense ferroelectric ceramics by Omatete in 1991. A ceramic powder, curing agent, solvent and dispersant are mixed together to form a homogeneous slurry. After in situ polymerization and demolding, the green bodies are sintered to obtain a dense ceramic. Recently, this method has been employed to manufacture porous ferroelectric ceramics by the addition of pore formers and decreasing the solid content of the ceramic slurry. Tert-butyl alcohol is often selected as the solvent and pore former since it has a high saturation vapor pressure and low surface tension force, which can be readily evaporated during the drying process. Gel spheres are formed after the polymerization process, and the gel spheres are then burnt out during the sintering procedure, and porous ferroelectric ceramics with spherical pores were obtained. Yang et al. fabricated porous PZT ceramics with three-dimensionally interconnected pores using the gel casting process. Interconnected pores, which were uniformly distributed, can be observed in Fig. 5b, where the pore shape is irregular with a pore size of around several microns.

Gel casting has attracted attention due to the simplicity and low cost. Furthermore, the porosity can be tailored in a wide range (20~70 vol.%), and the pore size can be adjusted from 3 to 350 μ m. It was demonstrated that porous ferroelectric ceramic fabricated by gel casting exhibited improved piezoelectric properties compared to those fabricated by burned out polymer spheres method, Yang *et al.* reported that the piezoelectric d_{33} constant was generally larger for samples fabricated by gel casting

compared to those formed by the burnt-out polymer spheres method, which was attributed to the more uniform and spherical pore structure induced by gel casting. However, tert-butyl alcohol is toxic and carcinogenic substance to the human body, therefore the application of gel casting is limited to a certain extent and there is potential for research to seek out alternative alcohol sources.⁸⁰

3.3 Freeze casting

Freeze casting is a method developed in recent 20 years to fabricate porous ceramics with complex pore structures.^{81,82} A freezing vehicle is used as a template, which is subsequently eliminated by freeze drying to generate pores. Firstly, ferroelectric ceramic powders are mixed with a freezing vehicle and additives to form a homogeneous slurry. Secondly, the ceramic suspension is poured into a mold and frozen in a specific temperature field. Then, the frozen liquid template is sublimated under a low pressure to freeze dry and remove the freezing vehicle. Finally, the porous dry samples are sintered to obtain porous ferroelectric ceramics. The microstructure and morphology of porous ceramics are dependent on the formulation of ceramic slurry, the freezing conditions and the types of freezing vehicle used. The porosity fraction can be controlled by solid loading of ceramic slurry, 3,84 and with an increase in solid loading the resulting porosity level is decreased. The freezing velocity can also be used to influence and tailor the pore size.⁸⁵ The porosity of porous ceramics fabricated by freeze casting usually ranges from 20 to 70 vol.%, and the pore size ranges from 3 to 100 μm .

The microstructure and morphology of porous ferroelectric ceramics fabricated by freeze casting primarily depend on the crystal morphology of the freezing agents. To

date, water, tert-butyl alcohol, and camphene are the mostly commonly used freezing agents. When water was employed as freezing agent, flat ellipsoidal pores were produced, and lamellar microstructures were formed. Branch-like connections were observed between the lamellar pores, since the morphology of ice crystal was dendritic. Porous ferroelectric ceramics fabricated by water-based freeze casting tend to be 2-2 type, with a nacre-like structure. Highly aligned one-dimensional pores can be obtained when tert-butyl alcohol was used, and the resulting pores are straight prismatic due to the acicular morphology of tert-butyl alcohol crystal. The resulting structure by this freezing agent can be thought as a 3-1 type connection (one dimensional pores in a continuous ceramic matrix).

Camphene has also been used as freezing agent to fabricate porous piezoelectric ceramics. The solidification of camphene results in formation of well-defined dendrites, leading to pores with a circular cross section^{3,4} The pore morphology of porous ferroelectric ceramics manufactured by freeze casting with different freezing agent is shown in Fig. 5c. Lamellar oriented pore structure are observed in water-based freeze casting, which shows a highly-aligned 2-2 type PZT-air composite connectivity. It can be noted that a three-dimensionally interconnected pore channels surrounded by thin PZT-PZN walls are formed when using camphene as a freezing agent. Guo *et al.* selected tert-butyl alcohol as a solvent to fabricate porous ferroelectric ceramics via freeze casting, where a aligned one-dimensional pore structure was observed. As a result, the morphology and pore structure can be controlled by selecting the appropriate freezing agent. However, each freezing agent has advantages and disadvantages.

Camphene can be frozen near room temperature and can be readily removed, but it is potentially flammable and toxic to humans. Tert-butyl alcohol can be frozen at around 25 □ and rapidly sublimates, nevertheless, it is flammable, toxic, cancerogenic and unfriendly to the environment. Water-based freeze casting is more environmentally friendly and low-cost, which is the most promising approach to fabricate porous ferroelectric ceramics.

Freeze casting has been considered as an attractive approach to obtain porous ferroelectric ceramics. It can provide a good processing flexibility to control the morphology, microstructure, and properties of porous ferroelectric ceramics. Moreover, a highly aligned pore structure can be acquired by freeze casting compared with other fabrication techniques. The porosity fabricated by freeze casting can be adjusted in a broad range, and allows high levels of porosity to be achieved. Most of the initial work on freeze casting examined non-ferroelectric ceramics, such as bioceramics, but it has been increasingly used to fabricate porous ferroelectric ceramics. For example, a hydroxyapatite/barium titanate porous ferroelectric scaffold was fabricated by freeze casting for bone tissue engineering. In addition, it has been demonstrated that porous ferroelectric ceramics manufactured by freeze casting possessed better properties than those formed by other methods, not only ferroelectric properties, but also mechanical properties, which will be discussed in detail in Section 4.

3.4 Replica template (polymeric sponge)

The replica template method can fabricate porous ferroelectric ceramics that duplicate the morphology and pore structure of the template used. In this approach, a

template is impregnated with a piezoelectric slurry, or sol-gel, and then the template is burnt out during the sintering process to produce a porous ferroelectric ceramic. 93,94 The selection of the template is important, since the morphology and microstructure is controlled by the template structure. The most commonly used template is a polymeric sponge, for example, polyurethane foam.⁹⁵ The properties of piezoelectric slurry should also be taken into consideration. To uniformly impregnate the polymeric sponge, the ceramic slurry is usually required to exhibit a pseudo-plastic or shear-thinning behavior. 6 In general, there is a squeezing procedure after the sponge is impregnated with the ceramic slurry. The main purpose of this procedure is to remove excess slurry after impregnation, which can also be used as an approach to control the volume fraction of ferroelectric ceramic. In addition, the volume fraction of ferroelectric ceramic can be increased by repeated impregnation of the template with the slurry of sol-gel. A sponge-like porous PZT ceramic skeleton was obtained by replica template method, and the template employed was a polyurethane foam.⁹⁷ The porous PZT ceramic skeletons feature interconnected pores with an average pore size of ~100 µm, which is similar to that of the natural sea sponges, as shown in Fig. 5d.

This approach can be used to create highly porous ferroelectrics, where the porosity of porous piezoelectric ceramics can be in excess of 80 vol.%, and pore size ranges from 100 to 300 µm. The advantage of the replica template method is that it can produce porous ferroelectric ceramics with high porosity, which could not be realized by the burnt-out polymer spheres method. Moreover, the pore structure, porosity and pore size can be readily adjusted by selecting polymeric templates with

the appropriate pore size, morphology, and fraction. However, a disadvantage of this method is the existence of pores and defect within the internal structure and struts of the porous skeleton, which stem from the volatilization of the polymer during the burnt-out stage. This can also lead to cracking of porous ferroelectric ceramic skeleton during the thermal decomposition of the polymeric sponge. The mechanical strength of porous ceramics formed by this route is therefore relatively poor due to the highly interconnected pore structure, the pores present within the internal structures of the ceramic struts, and the relatively large pore size.

3.5 Additive manufacturing

Porous ferroelectric ceramics fabricated via the above methods are often technologically limited when ferroelectric ceramics of complex geometries are required. In order to realize complex porous structures, intricate and fine-scale molds need to be designed and produced, which can be expensive and time-consuming. Additive manufacturing, as an emerging technique allows for the fabrication of complex structures without a mold, and can be employed to fabricate porous piezoelectric ceramics with a precisely controlled structure. There are seven major methods for additive manufacturing, of which direct ink writing is the most commonly used method to fabricate porous ferroelectric materials. Direct ink writing, which consists of a moving nozzle that dispenses ink onto a substrate layer by layer, has been utilized to produce piezoelectric materials with a complex 3D shape. Porous ferroelectric scaffolds with 3-1, 3-2 and 3-3 connectivities can be fabricated by direct ink writing.

ink writing, and subsequently infiltrated the structures with an epoxy to produce a PZTpolymer composites for hydrophone applications. Nan et al. fabricated macro-porous lead free ferroelectric scaffolds by direct ink writing. 105 Macroporous ferroelectric scaffolds with a woodpile structure have been fabricated by direct ink writing, as seen in Fig. 5e. 105 It can be seen that a wide range different fabrication techniques can be selected to obtain the desired porous structure. Moreover, porous ferroelectric composites can be manufactured by direct ink writing. For example, a porous piezoelectric composite manufactured from a polydimethylsiloxane (PDMS) containing Ag-coated PNN-PZT (0.55Pb(Ni 3 Nb 3)0 elastomeric matrix 0.135PbZrQ 0.315PbTiQ)ceramic heterojunction particles was fabricated by Wang et al. via direct ink writing. It was shown that the porous ferroelectric composite had potential for energy conversion and energy harvesting applications. ¹⁰⁶ In addition, fused deposition modelling and selective laser sintering have been used to manufacture porous ferroelectric scaffolds.²⁵,¹⁰⁷

There are many benefits of using additive manufacturing to create porous ferroelectric scaffolds. Firstly, structures with a wide range of shapes and geometrical complexity can be manufactured. Secondly, the microstructure and pore size can be readily controlled in a wide range (1 μ m \sim 10 mm). Porous ferroelectric scaffolds fabricated by additive manufacturing can exhibit multiple geometries, but any interconnected pores must rely on gaps between the printed lines, which are relatively coarse. As a result, the size of the generated pores is large and the integrity between layers can be poor.³⁰ Therefore, using additive manufacturing to fabricate ferroelectric

materials with excellent performance such as high hydrostatic voltage coefficient and energy harvesting figures of merit continues to face a number of challenges in further developing the processing technology.

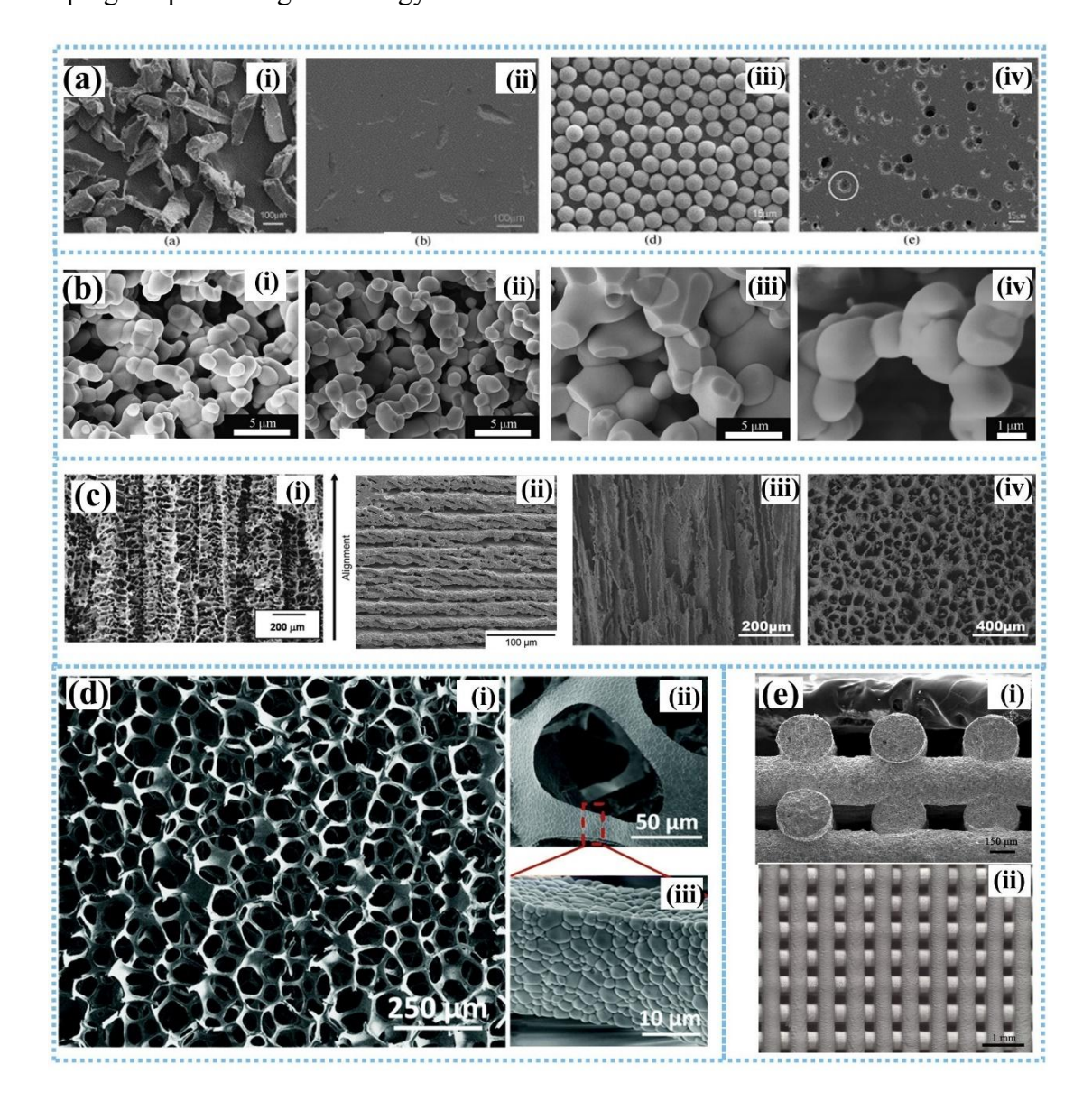


Fig. 5 Morphologies of porous piezoelectric materials obtained by different methods.

(a) porous PZT fabricated by burned out polymer spheres method by using spherical and irregular PMMA as pore-forming agents. Reproduced with permission. Copyright 2006, Elsevier. (b) porous PZT structure fabricated by gel casting. Reproduced with permission. Copyright 2010, Wiley-VCH. (c) aligned pore structures obtained via

freeze casting by using camphene, water, and tert-butyl alcohol as solvent. Reproduced with permission. Copyright 2008,2011,2015, Wiley-VCH. (d) sponge-like structure formed by replica template method. Reproduced with permission. Copyright 2018, Royal Society of Chemistry. (e) 3D printed porous BCZT skeleton. Reproduced with permission. Copyright 20018, Wiley-VCH.

4. Characterization and properties of porous ferroelectric materials

In Section 3, the fabrication techniques of porous ferroelectric materials were discussed, and porous ferroelectric materials with desirable pore structures can be obtained by selecting an appropriate manufacturing method. Since characterization can aid in understanding the properties, mechanisms and applications of porous ferroelectrics, the characterization and key properties of porous ferroelectric materials are systematically summarized in this Section, including the microstructure, dielectric, ferroelectric, piezoelectric, pyroelectric, and mechanical properties.

4.1 Microstructure

Ferroelectric domains have a close relationship with the crystal structure and ferroelectric properties of the material, which play an important role in the performance of perovskites. A number of studies have examined the domain configurations of dense ferroelectric ceramics, but less research has focused on the domain structure of porous ferroelectric ceramics. Xu *et al.* studied the domain configuration of porous PZT ceramics via scanning electron microscopy, where stripe domain patterns were clearly observed in the unpolarized grains. Compared with dense PZT ceramics, the domain

width of porous ferroelectric ceramics was smaller, which meant the domain walls can rotate more easily and respond actively to external electrical signals. Moreover, the poled pore wall of porous ceramics had better consistency in terms of domain direction, which is beneficial to piezo- and pyro-electric properties. Similar to Xu's research, Zhu et al. demonstrated that the domain size of porous piezoelectric ceramics was smaller than that of dense ceramics; where the domain size of the porous ceramic and dense ceramic were approximately 100-300 nm and 300-500 nm, respectively. The smaller domain size was attributed to the large surface area of the porous piezoelectric ceramics and the increased surface tension. 110 Tan et al. investigated the domain configuration of porous 0.36BiScO 0.64PbTiO ferroelectric ceramics by transmission electron microscopy, and the results showed that a nano-domain structure of approximately 7 nm was observed in an unannealed sample with a pore fraction of 9.4%. Furthermore, the domain size of porous 0.36BiScO 0.64PbTiO₃ ceramics decreased from 7 to 5 nm as the porosity fraction increased from 9.4 to 21.4%.111 Their work provided a deeper understanding of the domain configuration of porous ferroelectric ceramics. However, the study of domain structure of porous ferroelectric materials is still at an early stage, and more work should investigate the effect of pore structure on the domain configuration of porous ferroelectric materials and domain switching under the action of electrical and mechanical fields. Porosity can therefore provide an additional route to control the domain structure and domain kinetics of ferroelectrics to control the dielectric, piezoelectric and pyroelectric properties.

4.2 Dielectric properties

In terms of dielectric properties, the dielectric constant (relative permittivity), dielectric loss and dielectric temperature spectrum are often examined. For all investigated porous ferroelectric materials, the dielectric constant decreased with increasing frequency, since the ionic, space and spontaneous polarization cannot change in time with frequency, which is consistent with general ferroelectrics.¹¹² One significant feature of porous ferroelectric materials is that the dielectric constant can be reduced significantly, compared with dense ferroelectric materials, by introducing pores with a dielectric constant on unit; this reduced permittivity is clearly beneficial to a range of figures of merit outlined in eqn (1)-(5) for energy harvesting and mechanical or thermal sensing. A variety of studies have been shown that the dielectric constant decreased significantly with an increase of porosity, not only for ceramics, but also for ferroelectric polymers and composites.²⁶, 113 115 The sintering temperature can also affect the dielectric constant, where Zeng et al. indicated that the dielectric constant increased with an increase of sintering temperature due to the increased density and grain size of the ceramic regions? 1 The domain walls are more mobile in large grains and more dense ceramics, and the dielectric constant increases for materials with a high density and large grains.² 0

It was discussed in Section 3 that the burnt-out polymer spheres method is often used to fabricate porous ferroelectric ceramics. The type and shape of pore-forming agent can have an influence on the dielectric constant of porous ferroelectric ceramics. Bowen *et al.* used PMMA, PEO and self-raising flour (SF) as pore-forming agents, and found that PMMA based samples exhibited a lower permittivity due to the presence of

cracks perpendicular to the measurement direction that were introduced by uniaxial pressing.⁴² Du et al. employed PMMA and steric acid (SA) to fabricate porous ferroelectric ceramics, and their results showed that the dielectric constant of porous ceramic using PMMA as a pore-forming agent was higher than that using steric acid. The main reason was attributed to the porous microstructure and the grain structure.⁶³ The use of PMMA additives with spherical and an irregular shape was also studied, where it was observed that porous PZT ceramics with a spherical pore exhibit a higher dielectric constant compared to ceramics with irregular shaped pores.⁷ In addition to experimental results, several theoretical models have been developed to predict the dielectric constant of porous ferroelectric ceramics with a range of pore shapes. Banno et al. proposed a modified cube model to calculate the relative permittivity of porous materials, and the shape factor K_S was proposed (for spherical pores $K_S=1.0$, while for ellipsoidal pores, $K_S = 0.5$). Subsequently, it was found that this model is not suitable for some conditions, since the predicted values were not consistent with the experimental results. Based on this work, Du et al. proposed a modified semitheoretical and semi-empirical formula to predict the effective relative permittivity of the porous ferroelectric ceramics by considering effects of porosity, grain size (K_G) and pore shape (K_S) , which makes it possible to obtain a specified dielectric property by properly controlling the ceramic microstructure.⁶³

The pore orientation also plays an important role on the dielectric properties of porous ferroelectric materials. In general, pores generated by the burnt-out polymer spheres are randomly distributed. However, an aligned pore structure can be realized

by freeze casting and 3-1 type porous PZT ceramics were prepared via freeze casting by Guo et al. It was noted that the materials exhibited a higher dielectric constant compared to other types of porous PZT ceramics of the same porosity, which was due to the highly aligned one-dimensional pore structure formed by the freeze casting process. Moreover, different parts of the sample exhibited a different dielectric constant due to a change in the orientation level of pores at different locations.⁴⁴ Porous ferroelectric ceramics with various orientation angles of 0° , 45° and 90° respect to the poling direction were fabricated by camphene-based freeze casting. The orientation exhibited a higher dielectric constant compared to the material with a 0° material with a 90° orientation, since the alignment of pores in the poling direction resulted in an increase in the volume fraction and degree of interconnection of the piezoelectric material in the direction of interest. ⁸⁹ Zhang *et al.* fabricated unidirectional porous ferroelectric ceramics via water-based freeze casting and the dielectric properties of parallel-connected and series-connected structures were investigated. It was demonstrated that the dielectric constant of a parallel-connected structure was higher than that of series-connected structure, which was due to the improved interconnection in the parallel-connected freeze-casting PZT ceramic.¹¹⁷,¹¹⁸

The dielectric temperature spectrum of porous ferroelectric materials has been widely investigated. For ferroelectric ceramics, when the temperature is lower than Curie temperature (T_C), the dielectric constant increases with increasing temperature, which can be associated with an increase in polarization or conductivity. When the temperature is higher than the T_C , the relative permittivity of ferroelectric ceramics

reduces according to the Curie-Weiss law. 23,119421 The Curie temperature is an important parameter for ferroelectric ceramics and it represents a limit of operation for ferroelectric devices, and there have been various studies focused on the impact of porosity of the Curie temperature. Zhang et al. fabricated porous BCZT ceramics by the burnt-out polymer spheres method. As shown in Fig. 6a, the T_C increased slightly with an increase in porosity, which was attributed to stress relaxation near the pores.¹²² A similar trend was also observed in freeze-cast porous PZT ceramics, as shown in Fig. 6b. However, Stanculescu *et al.* reported that the T_C was almost unchanged with an increase of porosity and Lukacs et al. reported that the T_C decreased with increasing fraction of porosity.¹²³ It was also reported that the T_C of porous 0.36BiScQ -0.64PbTiQ ferroelectric ceramics decreased from 449 °C to 436 °C with an increase of porosity fraction, see Fig. 4c, which was attributed to the accelerated reversal of domains in the boundary of pores. 8 . Furthermore, Nie et al. showed that the Curie temperature remained almost unchanged with the increase of pore size, as shown in Fig. 4d. From the previous studies, it can be seen that there exist different responses with regard to the change of Curie temperature with porosity and further effort is needed to understand the mechanism by which porosity can change the T_c of ferroelectric materials.

There also are several studies on the dielectric loss of porous ferroelectric materials. It was reported that, at low frequencies, the dielectric loss of both dense and porous BCZT increased with a decrease in frequency, which is associated with a small contribution of conduction loss. At higher frequencies, the dielectric loss begins to

Furthermore, it has been shown that the dielectric loss of porous ferroelectric ceramics was higher than dense ceramics, and the dielectric loss increased with an increase in the porosity due to the increasing volume fraction of pores, which introduced a high dielectric loss in porous ferroelectric materials. The temperature dependence of porous ferroelectric ceramics was also investigated and it was found that the dielectric loss increased slightly with frequency when the temperature was lower than the T_C . However, the dielectric loss increased rapidly above T_C where it was thought that space charges gather at grain boundary and diffuse faster with increasing temperature, which led to an increase in dielectric loss! 26

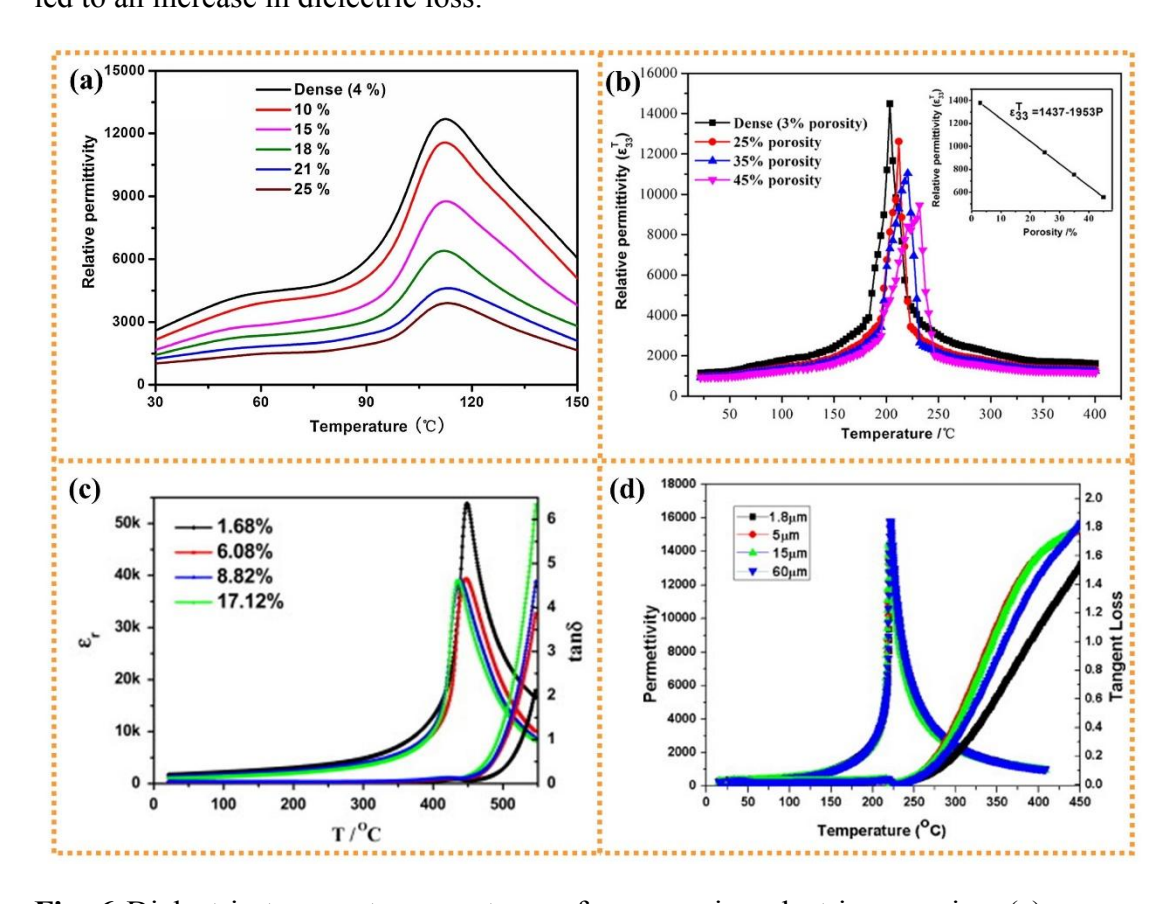


Fig. 6 Dielectric temperature spectrum of porous piezoelectric ceramics. (a) porous BCZT ceramics with different porosity. Reproduced with permission.¹²² Copyright

2019, Elsevier. (b) porous PZT ceramics with different porosity. Reproduced with permission. Reproduced with permission. Reproduced with permission. Reproduced with permission. Copyright 2015, Elsevier. (d) porous Pb 99 (Zr 95 To 05) 98 Nb 02 O ferroelectric ceramics with different pore size. Reproduced with permission. 24 Copyright 2011, Elsevier.

4.3 Piezoelectric properties

Measurement of the polarization (P) versus electric field (E) to measure a P-E loop is an important tool to characterize ferroelectric materials, whose shape can change with porosity. A number of studies have examined the P-E hysteresis loops of porous ferroelectric materials to obtain understand polarization reversal and determine the coercive field, remnant polarization, and saturation polarization.

Generally, the remnant polarization decreased with an increase in porosity due to the reduced amount of ferroelectric ceramic and the additional depolarization factor determined by the shape of the pore and the associated electric field distribution around the pore. Zeng *et al.* found that porous PZT ceramics with spherical pores exhibited a higher remnant polarization compared to porous PZT ceramics with irregular pores. Subsequently, Yap *et al.* fabricated porous BCZT ceramics using polyethylene (PE) microspheres and fibers as pore-forming agents, and their results showed that porous BCZT ceramics with elongated pores exhibited a lower remnant polarization than those with spherical pores, which can be attributed to the low electric field intensity around the pores during the polarization process. The orientation of pores also had an effect on the remnant polarization of porous ferroelectric materials. Zhang *et al.* compared the

remnant polarization of porous BCZT ceramic with randomly distributed pores and aligned pores, and it can be seen from Fig. 7a that the remnant polarization of the ceramics with aligned pores decreased more slowly with an increase in pore fraction compared to the randomly distributed pores.⁴⁵ In their next work, series-connected structure and parallel-connected structures with aligned pores were fabricated via a water-based freeze casting method. It was demonstrated that the parallel-connected structure exhibited a higher remnant polarization due to the lower fraction of low electric field and unpoled areas around the pores, compared with the series-connected structure, as seen in Fig. 7b. More detailed experiments were conducted by Schultheiß et al., in which the freeze-cast bodies at different angles ($\theta = 0^{\circ}$, 22.5°, 45°, 67.5°, 90°) with respect to the freezing direction were prepared. They found that the remnant polarization decreased with an increase in orientation angle, 27 which was related to the local electric field distribution within the porous microstructure, which on average both broadens and reduces in magnitude with increasing pore orientation angle. From the previous studies, it can be concluded that porous ferroelectric ceramics with parallelconnected structure had the highest remnant polarization.

Another important property that can be obtained from the P-E loops is the coercive field (E_c), which is a measure of the electric field required to switch the polarization direction of ferroelectric regions. A variety of studies have been conducted, but contradictory reports of the coercive field either increasing or decreasing with an increase of porosity have been reported. For example, Zhang $et\ al.$ showed that E_c increased with increasing fraction of porosity, whether the pores are random or aligned,

while Piazza *et al.* reported that the E_c decreased with an increase of porosity! ²⁸ These contradictory reports may be due to the factors such as the size of the pores, the pore distribution or introduction of defects. It has been summarized that E_c tends to decrease with increasing porosity irrespective of whether the pore morphology is random or aligned, when the porosity volume fraction is lower than $20\sim25$ vol%; this is thought to be due to presence of porosity leading to a more compliant ferroelectric matrix that facilitates domain motion and a lower coercive field. However, when the porosity volume fraction is higher than $20\sim25$ vol%, the coercive field tends to increase with increasing porosity fraction and this was due the more complex electric field distribution within the porous material and around the pores as a result of the contrasting dielectric constant of the high permittivity ferroelectric ceramic and the low permittivity air phase.

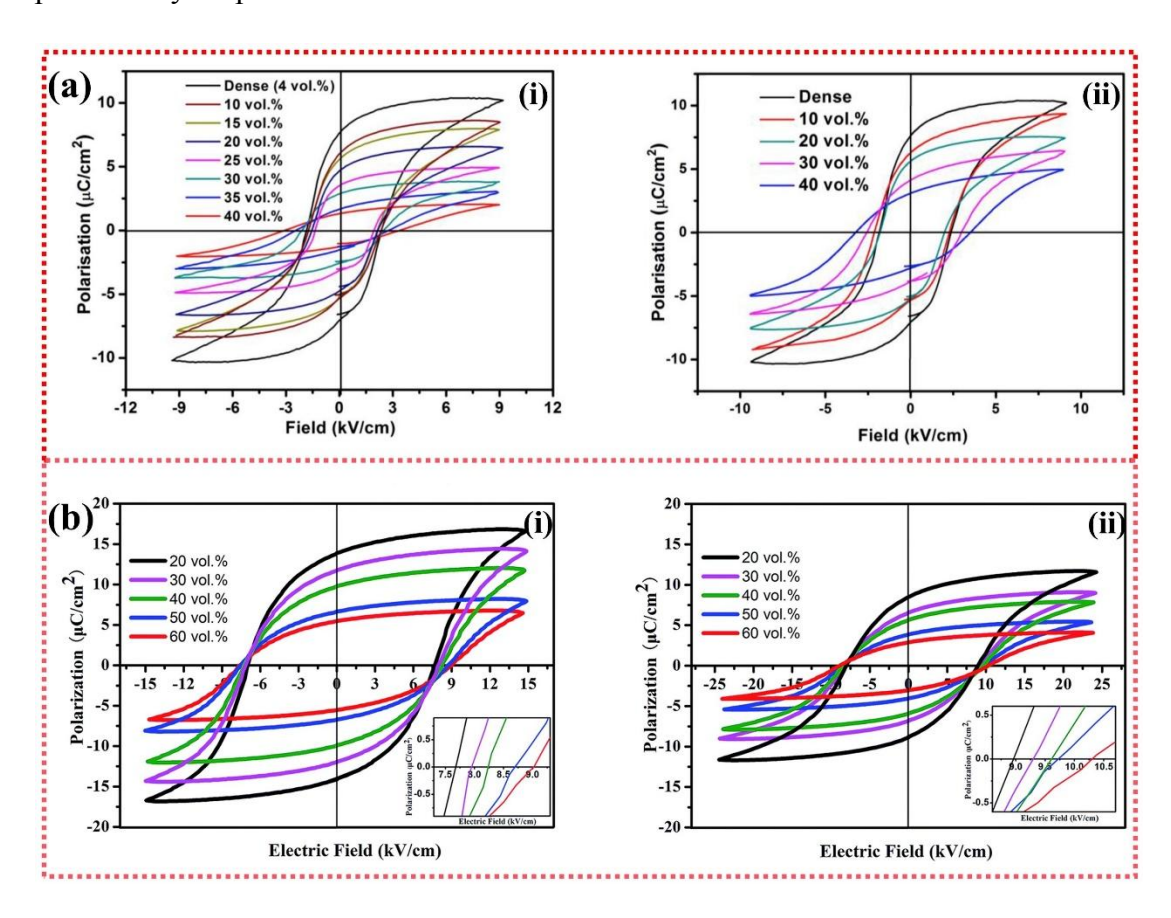


Fig. 7 P-E loops. (a) porous BCZT ceramics with randomly distributed pores and aligned pores. Reproduced with permission.⁴⁵ Copyright 2018, Elsevier. (b) porous PZT ceramics with series-connected and parallel-connected structure. Reproduced with permission.¹⁸ Copyright 2017, Royal Society of Chemistry.

The electric field induced strain is another crucial property of ferroelectric materials, since it is related to the actuation performance. Several researchers have examined the electric field induced strain of porous ferroelectric ceramics. It was reported that the electric field induced strain of porous ferroelectric materials was lower than dense materials, 66,110 and with an increase of porosity, the electric field induced strain decreased. The effect of pore size was also investigated, where it was seen that a larger pore size can decrease the strain of porous ferroelectric ceramics. 124 The effect of pore orientation angle on the strain was also studied. Similar to the observations on the P-E hysteresis loops, the electric field induced strain decreased with an increase of pore orientation angle. Interestingly, the bipolar and negative strain of porous ferroelectric ceramics with an orientation angle of zero were similar to the dense material, which indicates the potential for porous ferroelectrics as transmitters of acoustic signals or lightweight actuators, since the introduction of porosity can reduce the stiffness and acoustic impedance. However, the blocking force would also be reduced compared to dense materials due to the lower stiffness of porous ferroelectrics, so they may be more suitable for low-force actuation applications.¹²⁷ For acoustic projector applications, Butler derived a projector-transducer figure of merit (FoM_v) where $FoM_v \propto d_{ij}^2/s^E$ and s^E is the compliance at constant electric field.¹²⁹ The higher compliance of porous materials compared to dense materials leads to a lower projector figure of merit, although there are benefits of acoustic sensors.

The piezoelectric d_{ij} charge coefficients are of great importance to ferroelectric ceramics. A number of studies have been conducted to investigate the piezoelectric coefficients of porous ferroelectric materials. Generally, the longitudinal (d_{33}) and transverse $(-d_{31})$ piezoelectric coefficients decreased as the porosity fraction increased. The decrease in the piezoelectric coefficients can be ascribed to the reduced efficiency of the poling process, which leads to a reduced piezoelectric response 22 ; this stems from a decrease in the remnant polarization since due to the complex electric field distribution on porous ferroelectrics. The piezoelectric d_{ij} coefficients of porous ferroelectric ceramics are therefore usually lower than dense materials.

In addition, the introduction of pores improves the hydrostatic charge coefficient $(d_h = d_{33} + 2 d_{31})$. With regard to dense ferroelectrics, the value of $d_{33} \sim -2d_{31}$ and this results in small d_h coefficients. However for porous ferroelectrics, the magnitude of d_{31} decreases more rapidly than d_{33} , which leads to an increase of d_h with increasing porosity. Correspondingly, the hydrostatic voltage coefficient $(g_h = d_h/\varepsilon_0 \varepsilon_{33}^T)$ and hydrostatic figure of merit $(d_h g_h = d_h^2/\varepsilon_0 \varepsilon_{33}^T)$ are both increased due to a high d_h and relatively low permittivity. It can be observed that freeze casting generally leads to higher hydrostatic figures of merit compared to other fabrication techniques due to the highly aligned pore structure. The pore orientation also had an effect on the piezoelectric properties, and it was demonstrated that higher piezoelectric coefficients and hydrostatic figures of merit can be obtained when the pore orientation was parallel

to the poling direction. A very high hydrostatic figure of merit of 161 pm 1 N was obtained with porous PZT-PZN ceramics, which is due to the high porosity levels of these materials, $\sim 90 \text{ vol.}\%^{8.9}$

The piezoelectric energy harvesting figures of merit (FoM_{ij}) can be used to assess the capability of materials for mechanical energy harvesting, where there are several studies on the piezoelectric energy harvesting figures of merit. Shin et al. showed that the FoM_{ij} of porous sandwich structure increased first with increasing porosity, and then began to decrease at higher pore fractions. A 20 vol.% of the porous layer exhibited the highest piezoelectric energy harvesting figure of merit (FoM₃₃) of 4.53 pm N.¹³⁰ Moreover, it was demonstrated that the parallel-connected porous PZT fabricated by freeze casting exhibited a higher FoMii than the series-connected porous PZT. 118 Furthermore, the comparison of piezoelectric properties of porous ferroelectric materials is summarized in Table 1. It can be concluded that porous ferroelectric ceramics with an aligned pore structure formed by freeze casting exhibited superior piezoelectric properties such as d_{33} piezoelectric coefficient and hydrostatic voltage coefficient (g_h) compared with porous ferroelectric ceramics with randomly distributed pores. In addition, as can be seen in Table 1, most of the reported literature have examined PZT-based porous ceramics, and more work should be conducted on leadfree porous piezoelectric ceramics. Porosity can therefore be beneficial for the design and manufacture of lead-free porous ferroelectric materials in devices for piezoelectric energy harvesting and sensing applications.

Table 1. Comparison of piezoelectric properties for porous ferroelectric materials.

Method	Composite	Porosity	d_{33} (pC/N))	d_h (pC/N)	$g_h (10^{-3} \text{ Vm/N})$	$d_h g_h (10^{-12} \text{ m}^2/\text{N})$	Ref
BURPS	BCZT and air	10~25%	285~424	34~93	~10.2	~0.95	122
	PZT-PCN and air	24~45.6%	140~300	-	27~46	5.379	61
	PZT and air	35~54.5%	161~312	35~180	16.1~31.1	0.554~5.753	20
	PZT and air	35%	140	-	~175	~67	42
	PZT and air	5~45%	208~350	-	5~40	0.35~5	65
	LNKN and air	15~50%	75~153	-	-	-	35
	BS-0.64PT	17.12%	~485	-	2.4	~6.1	68
	PMN-PZT and air	33%	510	-	~19	4.8	22
	NKN and air	40%	~100	-	-	-	131
	BCZT and air	20%	381	-	-	-	130
	BT and air	30%	~124	-	-	-	132
	PZT and air	52%	-	~58	~57	-	126
Gel-Casting	PZT and air	27.8~72.4%	260~560	176~209	14.8~77.3	~15.2	78
	PZT and air	31.3~58.6%	424~635	-	-	0.81~10.1	24
Freeze-casting	PZT and air	$28.1\% \sim 68.7\%$	608~690	244~330	$8 \sim 28.3$	~9.7	90
	PZT-PZN and air	~90%	450	406	396	~161	89
	PZT-PZN and air	50~82%	380	259~298	34~118	9.5~35.65	34
	PZT and air	60%	-	~206	~83.5	~8.26	117
	PZT and air	20~60%	~350	-	-	-	118
	NKNS	~60.5%	~130	~60	~58.7	~3.5	92
	BT/HA	~55.6%	3.1	-	-	-	86
	BNT-6BT	~36%	182	-	-	-	110
Direct ink writing	PLZT	-	481	103	41	4.1	133
	PZT and epoxy resin	-	~360	~225	-	~4.8	104
	KNN	-	280	-	-	-	134

4.4 Pyroelectric properties

The pyroelectric properties of ferroelectric materials are important, since they are related to conversion of temperature changes into an electrical signal for sensing, or energy for harvesting. It has been reported the incorporation of porosity into a ferroelectric can be beneficial for pyroelectric applications, such as thermal sensors, detectors and imaging.¹³⁵

The relationship between pyroelectric coefficient (p) and porosity is relatively complex. With regard to porous BaSn 05 Th 95 Oceramics prepared using PMMA as pore-forming agent, it was found that the pyroelectric coefficient of the porous material initially increased with temperature and then began to decrease with an increase of temperature, which was similar to dense ferroelectric ceramics. As seen in Fig. 8a, the pyroelectric coefficient decreased with increasing fraction of porosity at the Curie temperature, due to the reduced amount of ferroelectric material and the additional polarization due to the presence of pores. There are important pyroelectric detection figures of merit to describe the performance of a material as a pyroelectric sensor; these including the current responsivity $(F_I=p/C_E)$ and the voltage responsivity $(F_V = p/\varepsilon_0 \varepsilon^T_{33} C_E)$. It can be seen that both the current and voltage responsivity increased for 2% PMMA content and thereafter decreased as the decrease in pyroelectric coefficient impacted to a greater extent on the figures of merit than the decrease in dielectric constant. The pyroelectric detection figures of merit of porous ferroelectric ceramics with aligned pore structure fabricated by freeze casting were also evaluated. It was observed that F_I remained almost constant with increasing porosity fraction for a parallel-connected structure, while there was a decrease in F_I with increasing porosity

for a series-connected structure. For F_V , the porous PZT for type of pore structure exhibited an increase in figure of merit due to the decrease in both C_E and ε^T_{33} ; it was shown that the series-connected structure had a larger F_V due to the lower dielectric constant.¹¹⁸

For thermal harvesting applications, the pyroelectric energy harvesting figure of merit $(F_E = p^2/\varepsilon_0 \varepsilon^T_{33}, F'_E = p^2/\varepsilon_0 \varepsilon^T_{33} C_E^2)$, where C_E represents the specific heat capacity) were evaluated. By adopting the freeze casting method, researchers studied the effects of aligned pore channels on the pyroelectric properties and an improved performance was realized in comparison to those with spherical pores.⁸ As shown in Fig. 8b, in the temperature range from 298 to 398 K, porous PZT ceramics exhibited higher energy harvesting figures-of-merit (F'_E and F_E) with an increase in porosity fraction at a specific temperature because the decrease in $\varepsilon_{33}C_E^2$ was greater than the decrease in p with increasing porosity. Furthermore, the pyroelectric energy harvesting performance of series-connected and parallel-connected porous PZT ceramics with aligned pore structure were investigated. The pyroelectric coefficient decreased in both types of freeze-cast PZT ceramics with increasing porosity fraction, and was lower than that of the dense PZT. As shown in Fig. 8c, the parallel-connected structure had a higher pyroelectric coefficient than the series-connected PZT at the same porosity due to the higher spontaneous polarization and improved poling of the parallel-connected configuration.

While the pyroelectric performance can be enhanced by introducing pores for specific figures of merit due to the reduction in permittivity and heat capacity, the

pyroelectric coefficient p tends to fall more rapidly with increasing porosity as compared to the piezoelectric d_{33} charge coefficient. This is primarily due to all the mechanical force being transferred to the high stiffness and active ferroelectric material in a porous structure, while a temperature change influences the whole porous structure, both the ceramic phase and the pore air phase. In addition, porous ferroelectric ceramics with aligned pore structure exhibited higher remnant polarization and poling efficiency than those with randomly distributed pores, which is beneficial for pyroelectric devices.

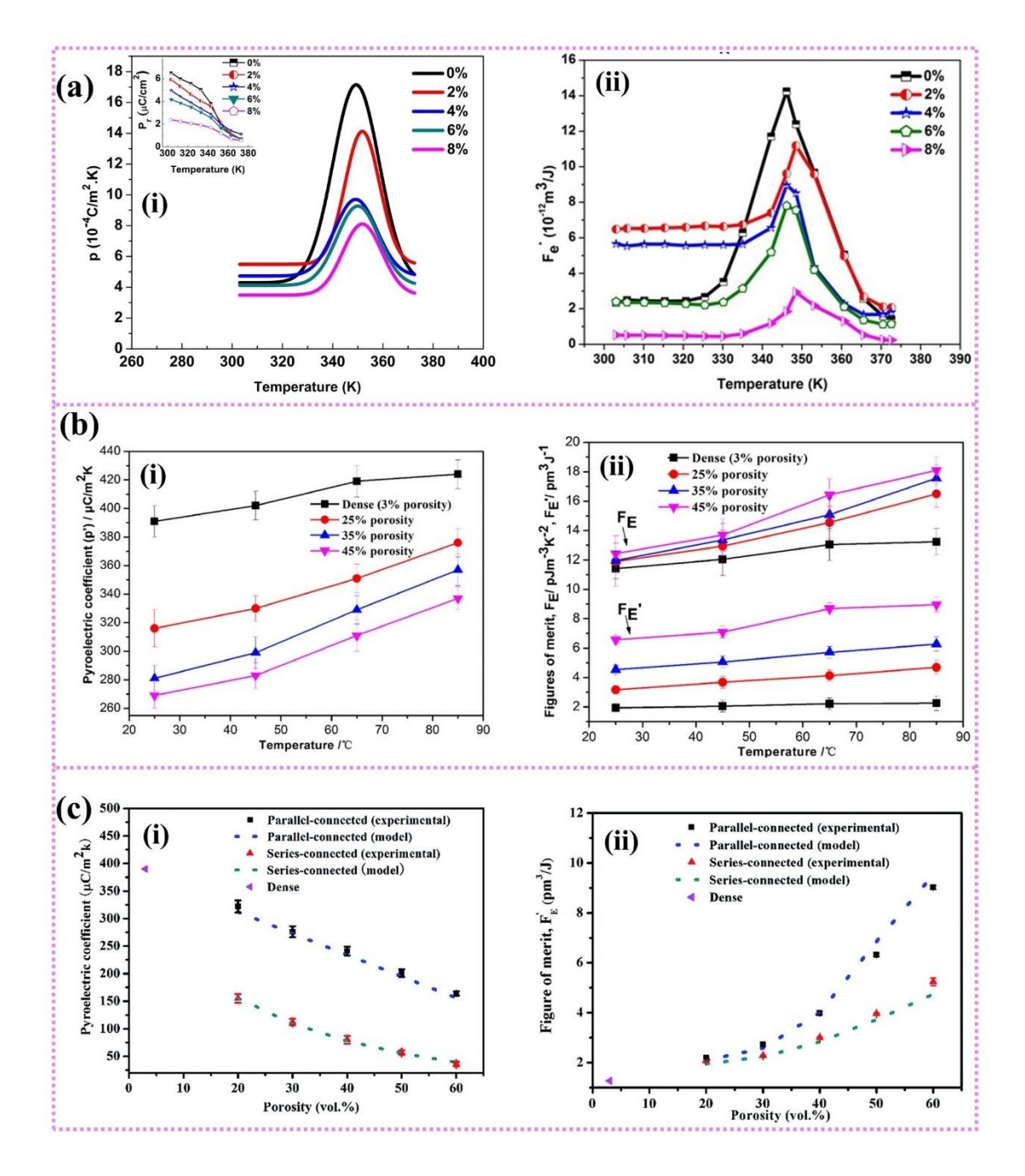


Fig. 8 Pyroelectric coefficient and pyroelectric energy harvesting figures of merit. (a) porous BaSn ₀₅ T₆₉₅ Oceramics. Reproduced with permission. Copyright 2017, Elsevier. (b) porous PZT ceramics with aligned pore structure. Reproduced with permission. Copyright 2015, Wiley-VCH. (c) porous PZT ceramics with seriesconnected and parallel-connected structure. Reproduced with permission. Copyright 2017, Royal Society of Chemistry.

4.5 Mechanical properties

The introduction of pores into ferroelectric ceramics is believed have a negative impact on the mechanical properties, as defects act as stress concentrators such that cracks are more easily to form when mechanical load is applied. A variety of studies investigated the mechanical properties of porous ferroelectric materials, including the stiffness and mechanical strength.

The porosity has the most direct influence on the Young's modulus of porous ceramics. Zeng *et al.* showed that the Young's modulus decreased with an increase of porosity. The effect of pore shape was also evaluated, where porous PZT ceramics with spherical pores exhibit a higher Young's modulus compared with porous PZT ceramics with irregular pores. Since the stress will be concentrated at the tip of irregular pores, it can also lead to poor mechanical strength. Pores can be beneficial to mechanical properties in some regard, where the acoustic impedance is of particular interest since it is relates to the stiffness and density. The acoustic impedance of a material is defined as the product of the density and the sound velocity (*Vs*).

$$Z = \rho V_{\rm s} \tag{6}$$

where Z is the acoustic impedance and is measured in 'rayl', ρ is the density and V_s is the sound velocity. The relationship between sound velocity, Young's modulus and density is given by eqn (7), where E is the Young's Modulus.

$$V_{\rm S} = \left(\frac{E}{\rho}\right)^{1/2} \tag{7}$$

Hence $Z = (E\rho)^{0.5}$, and clearly the introduction of pores in to a ferroelectric

reduces both the density and stiffness to reduce the acoustic impedance. Ramesh $et\ al.$ showed that the acoustic impedance (Z) of porous 3-3 piezoelectric composites decreases with an increase in porosity fractioh 37 and similar results were also obtained in porous PZT ceramics. The decrease of acoustic impedance can improve the impedance matching with water, air, biological tissue or low stiffness structures, which can improve the coupling of waves between piezoelectric generators, sensors, and the propagating media.

The mechanical strength of porous ceramics fabricated by different methods have also been studied. Zhang *et al.* reported that the freeze-cast porous PZT ceramics had a higher compressive strength than that of porous samples prepared by the burned out polymer spheres method due to the aligned pore structure. The pore orientation is believed to be another factor that influence the mechanical properties of porous ferroelectric ceramics. Porous PZT ceramics were prepared by water-based freeze casting, and the compressive strength was measured by changing the applied stress to the pore orientation. It was demonstrated that the compressive strength was 2.3 - 3.0 times higher than that vertical to the pore orientation, since the aligned pore structure in the direction of loading would help to carry and transfer the load through the porous ceramics.

In addition, the mechanical properties of porous ceramic-based ferroelectric composites have also been investigated where the pore space is infilled with a polymer phase. It was reported that a porous 3-3 interconnected composite had a high Young's modulus of 2.5 MPa compared to particle-based 0-3 type of BCZT composite.⁹⁸ Hao *et*

al. prepared 2-2 type PZN-PZT/PDMS composites via freeze casting, and the results showed that this structure had a high Young's modulus compared to pure PDMS and 0-3 type PZN-PZT/PDMS composite due to the existence of the interconnected skeleton structure that greatly improves stress transfer. Therefore, porous ceramic-based ferroelectric composites with aligned structure can exhibit improved mechanical properties.

5. Modelling of porous ferroelectric materials

In parallel with the development of experimental methods to synthesize and characterize porous ferroelectric materials, several modeling approaches have been developed to predict the properties of porous ferroelectric materials. Simulation data can be instructive for the design and manufacture of porous ferroelectric materials, therefore, the modelling of porous ferroelectric materials including analysis of the statistical electric field distribution, polarization-electric field response, dielectric, piezoelectric properties, and piezoelectric potential are summarized in this Section.

5.1 Modelling of electric field distribution

The poling process is crucial for achieving a remnant polarization in ferroelectric materials to provide a piezoelectric and pyroelectric response. Randomly orientated ferroelectric domains can be aligned when the applied electric field reaches a specific magnitude, known as the coercive field (E_c). For dense ferroelectric materials, the electric field distribution is relatively homogeneous so that materials can be almost fully poled at a specific electric field. However, the introduction of pores leads to an inhomogeneous electric field distribution, as the electric field will be concentrated in

the low permittivity pores as a consequence of Gauss' Law. 139141

Numerous studies have been conducted to investigate the electric field distribution of porous ferroelectric materials due to its significant effects on the poling process. The first factor that influences the electric field distribution is the porosity fraction. To demonstrate how the porosity affects the local electric field distribution, Gheorghiu *et al.* developed four different types of porous models with a range of porosity levels by 3D Finite Element Method (FEM). As shown in Fig. 9a, the electric field distribution was relatively homogeneous in a dense material since all regions within the microstructure exhibited the same dielectric constant. With an increase in porosity volume fraction, the electric field distribution became more inhomogeneous due to the introduction of the permittivity contrast between the low permittivity pores and high permittivity ferroelectric. Since there were local electric field concentrations in the pore regions, dielectric breakdown was also more likely to occur due with an increase in porosity fraction! 42

In addition to pore fraction, the other factor that influences the electric field distribution is the pore shape. Khachaturyan *et al.* developed two single-pore models with a variety of pore aspect ratios (namely spherical shaped pores and elliptical pores) using finite-element simulations to study the statistical electric field-distribution. A field-amplitude variation was observed due to the different permittivity of the ferroelectric matrix and the pores. The statistical field-amplitude ($f(E/E_m)$) around randomly distributed spherical pores was slightly higher than that of randomly distributed elliptical pores, which indicates that the presence of anisotropic shaped

pores in porous ferroelectric ceramics shifts the mean electric field towards smaller values, thereby decreasing the poling efficiency.¹⁴³

Ayuso et al. investigated the influence of pore shape on the electric field distribution at a microstructural scale using finite element modelling. As shown in Fig. 7b (upper figures), the electric field was prone to clustering at the top and bottom of the pore (poles C and D), which were aligned perpendicular to the electric field direction. In contrast, weakened electric fields were observed at the right and left sides of the pore (poles A and B) which were one sixth of those at the top and the bottom of the pores. On increasing the pore aspect ratio in a direction perpendicular to the poling direction, it can be observed in Fig. 9b (lower figures) that the electric field distribution became more inhomogeneous and the difference between the electric fields at the top/bottom and the left/right hemispheres reached up to a factor of ten, which was attributed to the point discharge effect on high-curvature areas. Thus, it can be concluded that the introduction of high-aspect-ratio pores orientated perpendicular to the poling direction could result in an anisotropic electric field distribution and lead to a lower number of polarized elements compared with spherical pores under the same applied electric field144

Yap *et al.* also simulated the electric field distribution of porous ferroelectric ceramics (BCZT) with ellipsoid pores, but in contrast to the above research, their long axes were parallel to the poling direction. As shown in Fig. 9c, the electric field distribution tended to be disrupted around the pores, leading to regions of low and high electric field intensities around the pores. Similarly, low electric fields were observed

on the two hemispheres parallel to the poling direction. Interestingly, highly homogeneous electric field distributions were detected at both sides of most pores perpendicular to the poling direction, which may be due to the relatively low local curvature. In addition, the electric field distribution concentrated on the pore walls between two pores, which were very close to each other, as marked in the box in Fig. 9c. Thus, it can be concluded that the highly inhomogeneous electric field distribution was a result of the introduction of low permittivity pores, and could be inhibited if the curvature of the edge perpendicular to the poling direction is sufficiently low.

An outcome of these analyses is that one approach is to consider a structure where the pores are perpendicular to the poling direction, or the aspect ratio of the elongated pore reaches extremely high values to positive infinity. A porous three-dimensional model with an idealized 2-2 structure was therefore developed, and the results were shown in Fig. 9d. It can be seen that the electric field distribution in the ferroelectric phase moved to lower magnitudes with increasing porosity fraction, therefore, a larger electric field needs to be applied to achieve domain switching during the poling process. A similar electric field distribution with an increase of porosity content was demonstrated by Zhang *et al.*, where a randomly distributed pore structure model and aligned pore structure model were analyzed. The results showed that the electric field of the porous structure with randomly distributed pores was much lower than porous ceramics with pores aligned in the polarization direction, and the electric field distribution around the aligned pore channel was highly homogeneous, which indicated that porous ferroelectric ceramics with aligned pore structure are more easily poled;

this would lead to improved level of poling and higher piezoelectric and pyroelectric properties.⁴⁵

Another factor that may influence the electric field distribution is the pore orientation angle. Roscow *et al.* developed a single elliptical pore with a constant area fraction to investigate the effect of pore orientation angle, in which the angle of the pore was varied from 0° to 90°. As shown in Fig. 9e, regions of low electric field intensity are present in the ferroelectric phase in the immediate vicinity of the pore at the poreceramic interfaces located perpendicular to the applied field. With an increase of pore orientation angle, more of the ceramic became unpoled due to low electric field intensity above and below the pore! ⁴⁵ The electric field distributions with highly-aligned porous PZT ceramics fabricated by freeze casting with different angle were also studied. It can be noted that the local electric field distribution shifted towards lower electric fields and became broader with increasing pore orientation angle. Therefore, more complete polarization can be achieved by aligning high aspect pores parallel to the poling direction! ²⁷

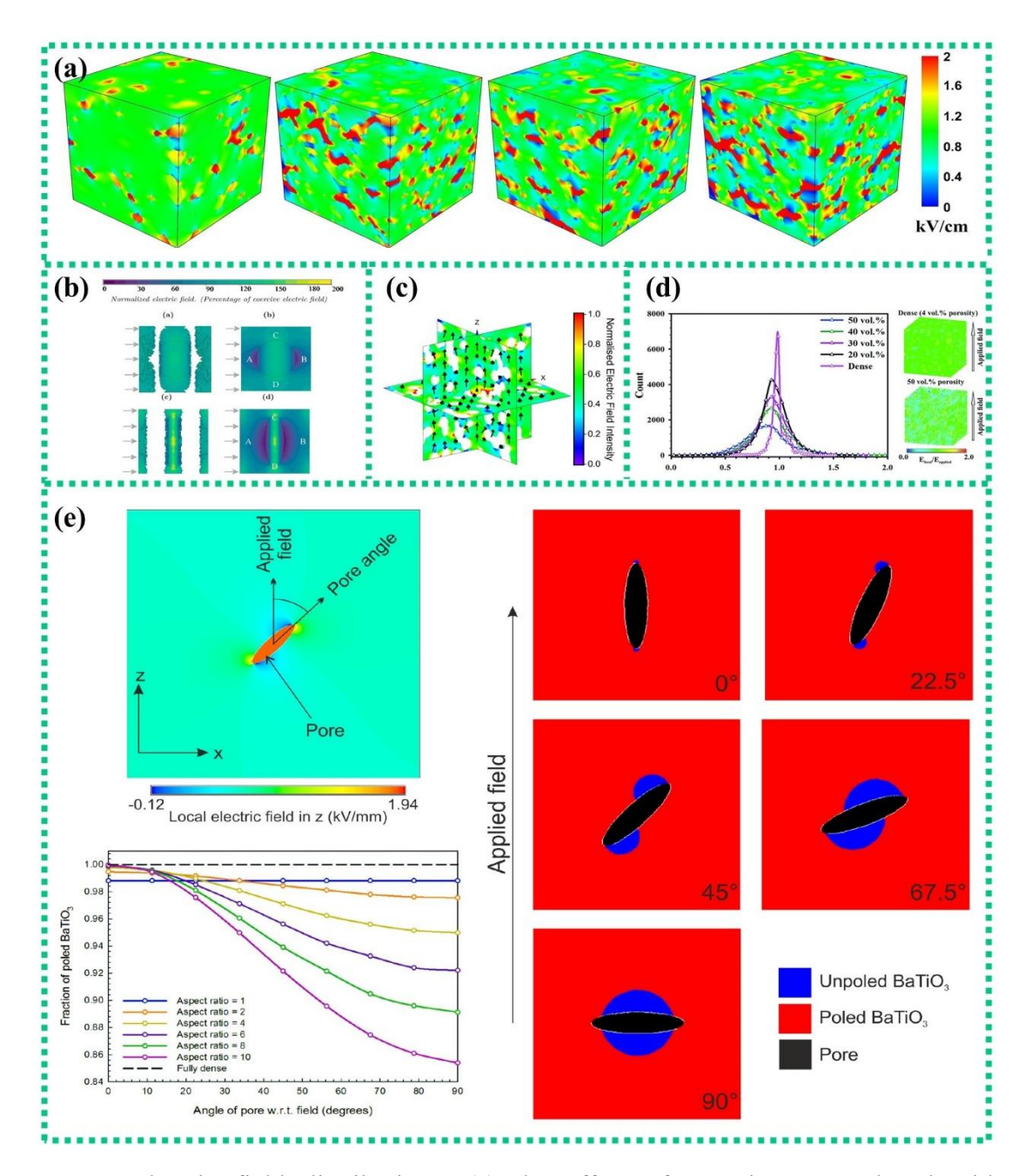


Fig. 9 Electric field distributions. (a) the effect of porosity. Reproduced with permission. Permission. Wiley-VCH. (b) comparison of spherical pore and elliptical pore. Reproduced with permission. Permission. Elsevier. (c) porous BCZT ceramics fabricated by using PE spheres and fibers as pore-forming agents. Reproduced with permission. Elsevier. (d) porous PZT ceramics with aligned pore structure. Reproduced with permission. Copyright 2018, Elsevier. (d) porous PZT ceramics with of Chemistry. (e) the effect of pore angle and pore aspect ratio. Reproduced with

5.2 Modelling of polarization-field loops

The polarization-field (*P-E*) loop contains the shape of the hysteresis loop, remnant polarization and coercive field, which ultimately affect the final piezoelectric and pyroelectric properties of a porous ferroelectrics. Thus, for porous ferroelectric materials and composites, it is meaningful to understand the correlation between these properties and the pore-structure.

The shape of hysteresis loop of porous ferroelectric materials is firstly discussed. Zhang *et al.* simulated polarization- electric field loops by applying a voltage profile withing a model, similar to those applied in the experimental measurements. Both randomly distributed pores and aligned pores were simulated. As shown in Fig. 10a, the ferroelectric ceramic regions remained unpoled when the applied electric field was lower than the coercive field. However, with an increase in electric field, the ferroelectric materials gradually became poled, since polarization switched from an unpoled state to a positively poled due to increase in applied electric field; finally the ceramics were fully poled. Then, the polarization was switched from positive to negative state as the applied electric field was revered, until the ceramics became fully poled in the reverse direction.

The polarization-field loops exhibited increased tilting, and the remnant polarization decreased with increasing porosity, which was in agreement with the experimental data. The decrease in remnant polarization with increasing porosity stems from the reduction in the amount of material due the porosity and the additional

depolarization factor due to the unpoled regions around the pores, as shown in Fig. 10b. In addition, the rate of the decrease in remnant polarization with increasing porosity fraction was higher for the randomly distributed porous structures compared with the aligned porous structures.

The variation of coercive electric field for the two types of structures was also evaluated. As shown in Fig. 10c, the coercive field for the randomly distributed porous structure increased with an increase in porosity fraction, although not as fast as the experimentally measured data. Again, this increase in coercive field was due to the broadening of the electric field distribution due the presence of low permittivity pores. However, the aligned porous structure showed little change in coercive field with increasing porosity fraction since the electric field distribution to lower due to existence of high aspect ratio pores. The modelling of the polarization-field loops provided a detailed understand of the poling process of porous ferroelectric materials and the impact of porosity on remnant polarization and coercive field. As a result, the introduction the presence of porosity provides additional control over the internal electric field and domain switching in ferroelectric materials.

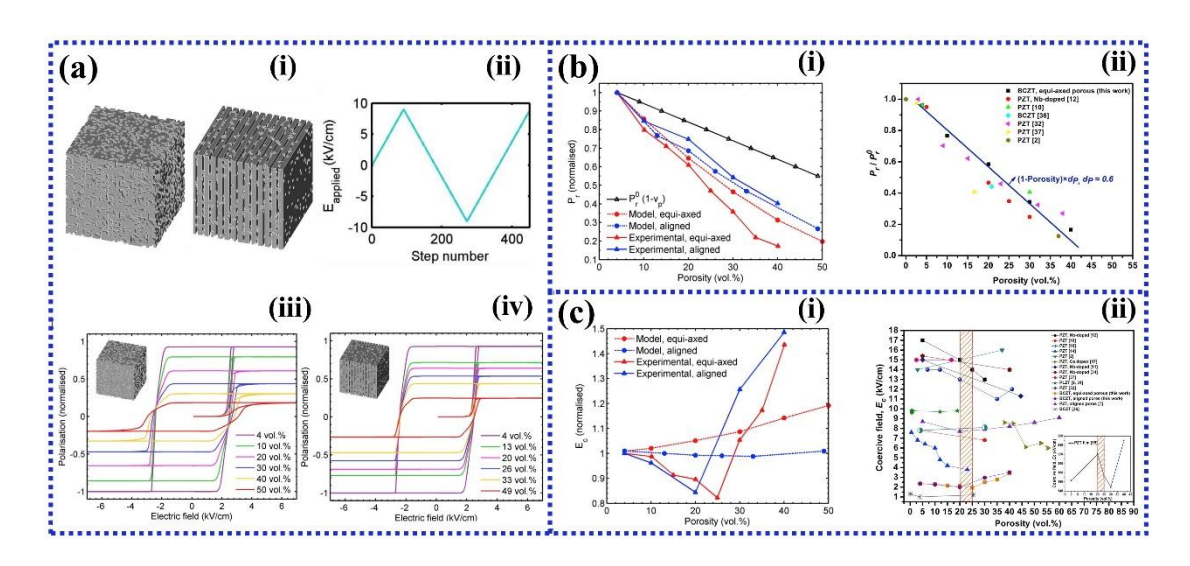


Fig. 10 (a) schematic of the model and simulation of polarization – electric field (P-E) loops. (b) simulation of remnant polarization. (c) simulation of coercive field. Reproduced with permission.⁴⁵ Copyright 2018, Elsevier.

5.3 Modelling of dielectric and piezoelectric properties

A number of studies have been conducted to investigate the dielectric and piezoelectric properties of porous ferroelectric materials through analytical modeling, numerical modeling, and finite element modelling. Kar-Gupta et al. developed a finite element model to study the effect of porosity on 3-1 type porous ferroelectric materials. It was demonstrated that the dielectric constant and piezoelectric charge coefficient decreased monotonically with an increase in porosity volume fraction. The hydrostatic figure of merit also exhibited moderate increase with porosity. As Bosse et al. developed three-dimensional finite element models to characterize the effect of microstructural features to the piezoelectric and dielectric properties of 3-3 type piezoelectric foam structures. The piezoelectric figures of merit, such as the hydrostatic piezoelectric charge coefficient (d_h) , hydrostatic piezoelectric voltage coefficient (g_h) and the hydrostatic figure of merit $(d_h g_h)$ can be enhanced significantly by modifying the aspect ratio of the porosity. ⁴⁷ Moreover, three kinds of 3-3 type piezoelectric foam structures (i.e. with asymmetric interconnects, with symmetric interconnects, and without any interconnects) were created by Challagulla et al. The longitudinal dielectric constant of the 3-3 open foam structures was lower than the 3-1 type long porous structure, while the transverse dielectric constants were higher in the open foam structures. The piezoelectric constant of the 3-3 type open foam structures were lower than that of the

3-1 type long porous structure. The highest piezoelectric coupling constants and the highest acoustic impedance were obtained in the interconnect-free (3-3 type) piezoelectric foam structures. In addition, Ayuso *et al.* studied the effect of pore shape on the dielectric and piezoelectric properties of porous ferroelectric materials. The dielectric constant showed an almost linear dependency with respect to the porosity fraction for both spherical and ellipsoidal models. The piezoelectric charge coefficients decreased with increasing porosity fraction, while the piezoelectric coefficients of the ellipsoidal model fell faster than that of the spherical model owing to the less poled regions and the electric field distribution around the pores.

5.4 Modelling of piezoelectric potential

Ferroelectric materials are able to generate an open circuit electric potential when an external stress is applied due to the direct piezoelectric effect. Therefore, ferroelectric materials can be used as sensors and energy harvesters. We have seen that the introduction of pores can enhance the sensitivity (voltage per unit stress) and energy harvesting performance (energy density per unit stress); see also eqn (1) and (4). Research has investigated the open circuit electric potential generated by porous ferroelectric materials using finite element methods. Zhang *et al.* simulated the electric potential of porous PZT microfoams using phase field simulations. The porous PZT skeleton was modelled as an isotropic elastic material with the poling direction normal to the surface of the porous composite, while the PDMS within the pores was modeled as an isotropic elastic material with no piezoelectric properties. As shown in Fig. 11a, the calculated output voltages are 21 V, 52 V, and 84 V at 2%, 5%, and 8% applied

strains, respectively, which is in good agreement with the experimental results.⁹⁷ Phase field computation was used to simulated the electric potential of a sea sponge-inspired BCZT porous composite and a randomly dispersed BCZT particle-based composite. It can be seen from Fig. 11b that the generated electric potential of 3D interconnected composite is approximately four times higher than that in a random particle composite due to the enhanced stress transfer into the active piezoelectric material due to the interconnected structure. 8 Similarly, Zhang et al. compared the stress and piezoelectric potential distribution of 3D interconnected Sm-PMN-PT composite and a Sm-PMN-PT nanoparticle composite using the phase-field simulation with a Fourier spectral iterative perturbation method. It can be noted that a higher stress transfer was observed in the 3D composite, which led to the generation a higher open circuit potential. ¹⁴⁹ In addition, Hao et al. investigated the distribution of stress and piezoelectric potential of a freezecast 2-2 type porous composite and a 0-3 composite. As shown in Fig. 11c, the freezecast 2-2 type composite showed a higher applied net stress and stronger piezoelectric potential. 138 It can be concluded from the results of modelling that porous ceramicbased ferroelectric composites with a 3-3 or 2-2 structure can generate a higher piezoelectric potential compared to a 0-3 structure, which exhibited potential for both sensing and energy harvesting applications.

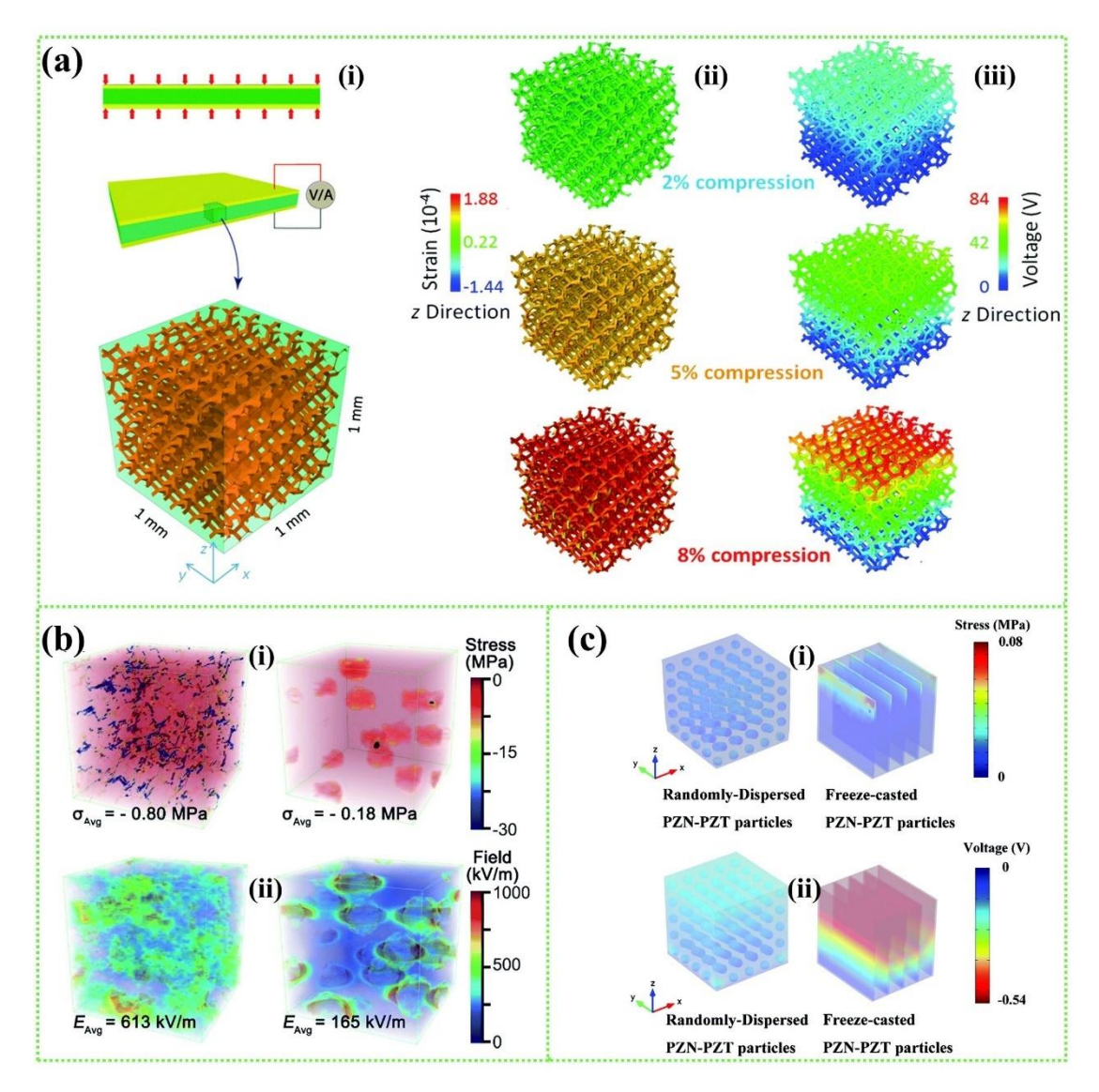


Fig. 11 Electric potential and stress distribution. (a) PZT microfoams under different strain. Reproduced with permission. Copyright 2018, Royal Society of Chemistry. (b) porous BCZT composite and random particle composite under 12% compressive strain. Reproduced with permission. Copyright 2018, Royal Society of Chemistry. (c) freeze-casted 2-2 type porous PZT composite and 0-3 type PZT composite. Reproduced with permission. Copyright 2020, Elsevier.

6. Applications of porous ferroelectric materials

Ferroelectric materials can be applied as energy harvesters, sensors, and catalysts due to the *direct* and *converse* piezoelectric effect. Compared with dense ferroelectric materials, porous ferroelectric materials possess many benefits, such as relatively high piezoelectric d_{33} charge coefficients and pyroelectric coefficient p, high d_h coefficients, high surface area A, low relative permittivity ε_{33}^T , and low specific heat, leading to enhanced piezoelectric energy density, hydrostatic sensitivity, pyroelectric sensitivity and improved piezo- or pyro-catalysis performance, as described in Fig. 12. These benefits make porous ferroelectrics attractive candidates for the applications of energy harvesting, sensing and catalysts. However, the actuation performance of porous ferroelectric materials is not improved compared with dense materials, and the applications of porous ferroelectric materials for actuators are less attractive. Therefore, the applications of porous ferroelectric materials for energy technologies are summarized in this section, including energy harvesting, sensing, and catalysis.

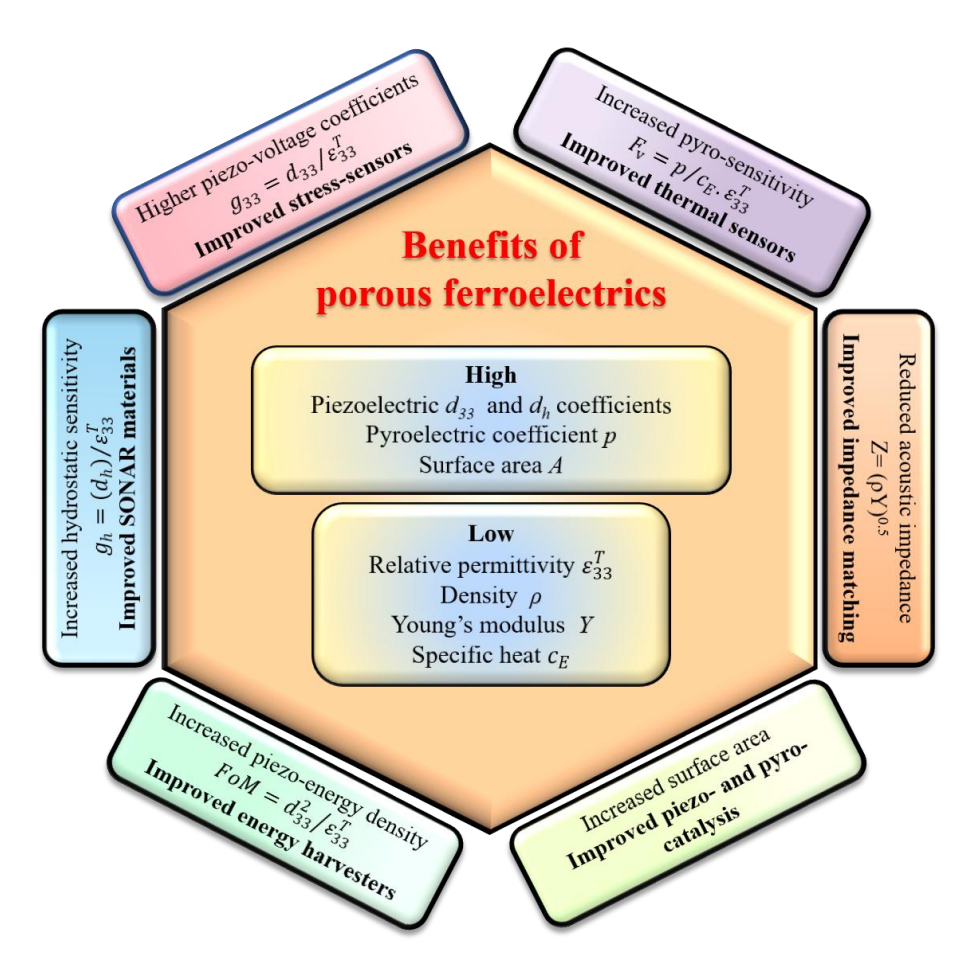


Fig. 12 Benefits of porous ferroelectrics and their potential applications

6.1 Energy harvesting

Many energy sources in our living ambient environment can be converted into usable forms, such as electrical power, through energy harvesting to supply power for low power electronic devices. Compared with a conventional battery-powered device, this enables the device to be self-powered and wireless, with potential for reduced maintenance costs. In particular, ferroelectric materials are good candidates for energy harvesting due to their ability to convert mechanical vibrations or temperature fluctuations via the piezoelectric effect and pyroelectric effect as well as the high energy density, which can exceed electromagnetic generators at dimensions below 0.5 cm ? 1

6.1.1 Piezoelectric energy harvesting

Piezoelectric energy harvesting can capture ambient mechanical vibration energy and convert it into electric energy via the *direct* piezoelectric effect. It can be seen from eqn (1) that the harvested energy is highly dependent on the piezoelectric charge coefficient and the dielectric constant, which means that more energy can be obtained from ferroelectric materials with higher piezoelectric charge coefficient and lower dielectric constant. The introduction of porosity can significantly reduce the dielectric constant, while the piezoelectric charge coefficient decreases slowly with increasing porosity. Previous studies have demonstrated that porous ferroelectric materials possessed higher piezoelectric harvesting figure of merit than dense materials.¹¹⁸ Therefore, porous ferroelectric materials exhibit potential for piezoelectric energy harvesting applications. Many researchers have employed porous ferroelectric materials to harvest mechanical energy, including porous ferroelectric ceramics, polymers, and composites. Roscow et al. used porous barium titanate ceramics fabricated by freeze casting to harvest vibration energy. The maximum measured voltage across the charged capacitor was found to be 234 mV for porous ceramic with 45 vol.% porosity compared with 96 mV for dense barium titanate. Porous sandwich structures based on BCZT ceramics were investigated for energy harvesting applications, the sample with a 20 vol% of the porous layer had an output voltage of 3 V and energy density of 7.29 mJ/cm ¹³⁰

Due to the brittle nature of ceramics, its low fracture toughness greatly limits their applications for energy harvesting. Thus, porous ferroelectric polymers have attracted much interest due to the good flexibility and enhanced electromechanical coupling

efficiency. The most commonly used ferroelectric polymers are PVDF and its copolymers. Chen et al. fabricated porous PVDF-TrFE film by a phase separation method and used it for energy harvesting, the maximum generated voltage reached to 5.1 V^{5.0} A sponge-like porous PVDF film was fabricated by Mao *et al.* via an etching template method and was used as an energy harvester. As shown in Fig. 13a, the maximum output voltage was 11.5 V with the porosity of 50 vol.% at 60 Hz and the output power reached 0.16 mW/cm at 60 Hz. 50 Similarly, a high-performance porous piezoelectric nanogenerator based on PVDF was prepared by the same method. A peakto-peak open-circuit voltage of 84.5 V and a peak output power density of 41.02 μW/cm were obtained when the device was excited using a linear motor shaking at 30 Hz^{151} Moreover, porous Ag/PVDF-TrFE piezoelectric composites using ZnO nanoparticles (NPs) as the template were fabricated by Zhou et al., which exhibited a high output power density of 7.1 μ W /cm as shown in Fig. 13b. An enhanced electrical energy generation in a porous PVDF-HFP was achieved via coupled piezoelectric and dielectric processes, see Fig. 13c. 153 In addition, a piezoelectric and triboelectric hybrid nanogenerator based on PANI/PVDF-TrFE porous aerogel was fabricated by Yu et al. via freeze drying and liquid nitrogen quenching methods. It can be seen from Fig. 13d that the optimal output reached 246 V and 122 µA at a frequency of 30 Hz and pressure of 0.31 MPa, and the power density is calculated to be 6.69 W/m . 154 This type of porous ferroelectric polymer provided a new strategy for energy harvesting applications.

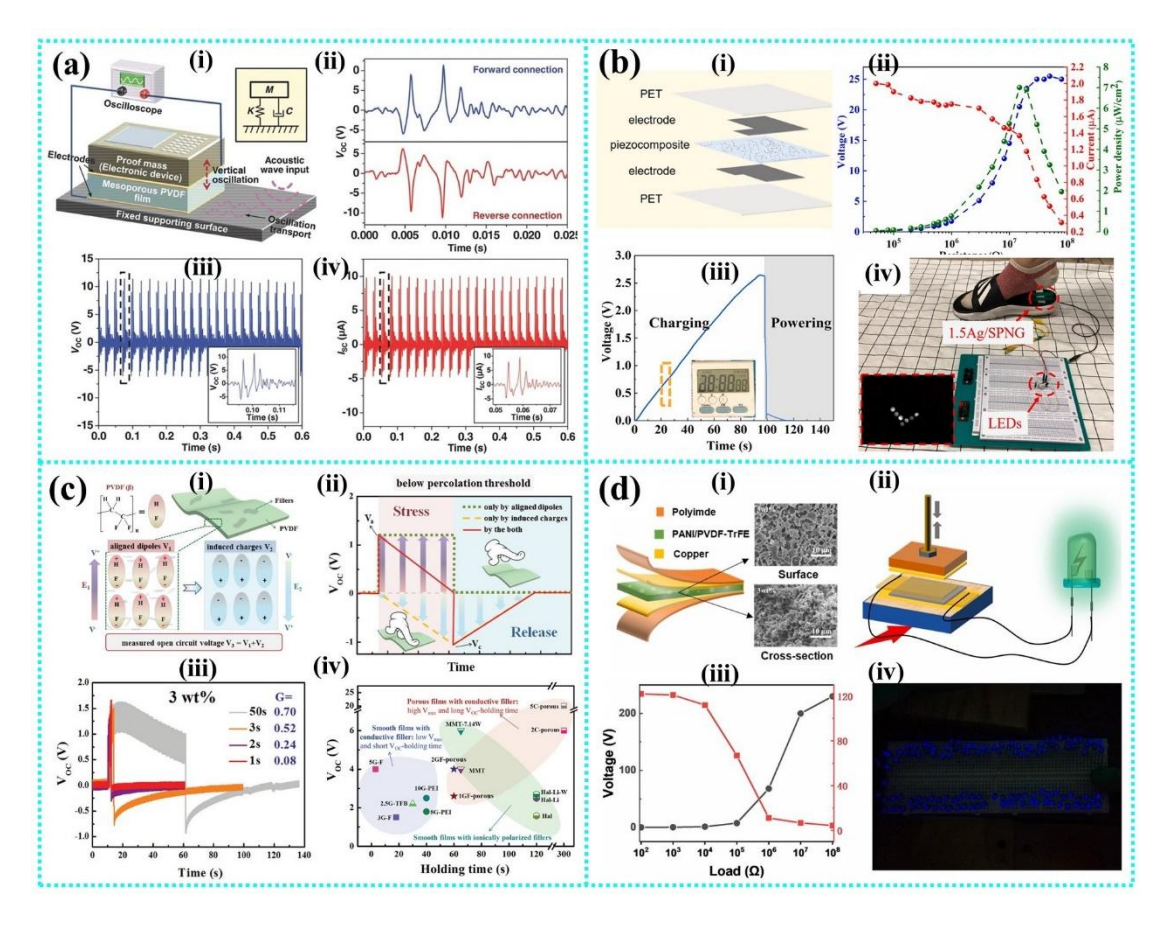


Fig. 13 Piezoelectric energy harvesting applications. (a) output voltage and current of sponge-like PVDF porous film. Reproduced with permission. Copyright 2014, Wiley-VCH. (b) voltage and power of Ag/PVDF-TrFE piezoelectric composite. Reproduced with permission. Copyright 2021, Elsevier. (c) energy harvesting performance of porous PVDF-HFP film. Reproduced with permission. Copyright 2020, Wiley-VCH. (d) voltage and power of PANI/PVDF-TrFE aerogel. Reproduced with permission. Elsevier.

Porous ceramic-based ferroelectric composites, which consist of a porous ferroelectric skeleton and a polymer within the pore space, have been shown to be promising candidates for piezoelectric energy harvesting due to their high energy harvesting figures of merit and high flexibility. A number of researchers have used 3-3 type of porous piezoelectric composites for energy harvesting. For example, Zhang *et*

al. designed 3-3 type piezoelectric composite generators based on a three-dimensional BCZT ceramic skeleton. As shown in Fig. 14a, the open-circuit voltage, short-circuit current density and instantaneous power density of the energy harvester reach up to 25 V, 550 nA /cm and 2.6 mW /cm, respectively. 98 Likewise, a flexible piezoelectric composite generator based on a 3D Sm-PMN-PT interconnected piezoceramic was developed. The maximum instantaneous power density was 11.5 μW/cm which is ~ 16 times higher than that of the conventional nanoparticle-based composite due to the effective stress transfer ability, see Fig. 14b. 149 As shown in Fig. 14c, a porous piezoelectric scaffold was fabricated via direct ink writing which could drive over 20 commercial red-LEDs lighting directly without using a charge storage capacitor. 106 More recently, 2-2 type porous piezoelectric composites have attracted much attention, where Hao et al. fabricated a 2-2 type PZN-PZT/PDMS harvester. Fig. 14d shows that the measured output open-circuit voltage and short-circuit current density were ~25 V and ~170 nA/cm respectively! 38 A piezoelectric energy harvester based on a gradient porous PZT/PDMS composite has also been developed, where the generated voltage and current could reach 152 V and 17.5 mA, and a corresponding instantaneous power of 1.1 mW illuminated 96 commercial LEDs, see Fig. 14e. Subsequently, Yan et al. designed a novel lead-free flexible piezoelectric energy harvester structure based on porous BCZT pillars and PDMS, as shown in Fig. 14f. The output voltage and current generated by a piezoelectric composite formed using a ceramic with 60 vol.% porosity could reach as high as 30.2 V and 13.8 µA, respectively, with the maximum power density of 96.2 μWcm^{2} . This work demonstrated the potential application of porous

piezoelectric composites in energy harvesting. More research should be conducted to further optimize the porous structure and device design for piezoelectric energy harvesting.

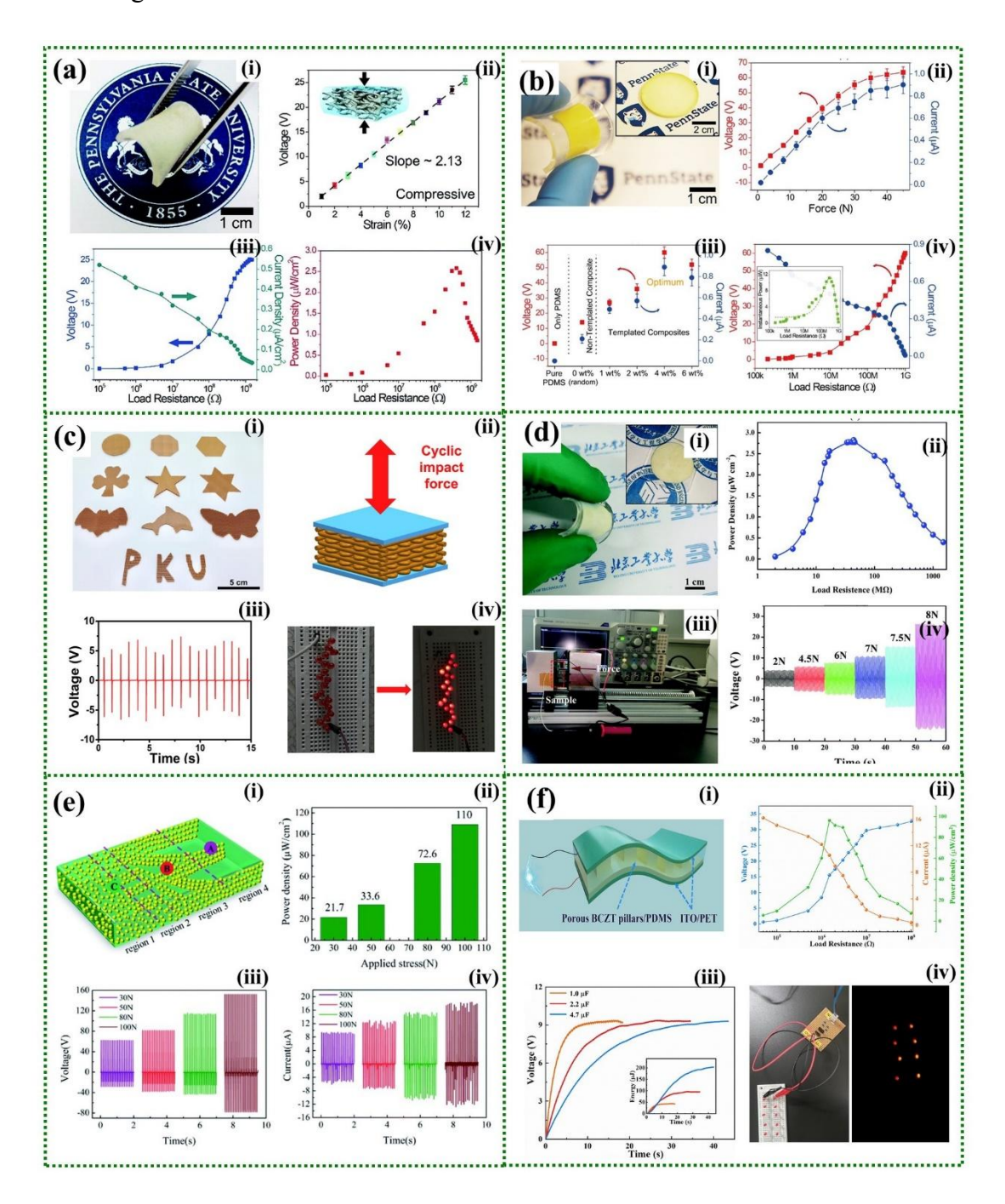


Fig. 14 Piezoelectric energy harvesting applications. (a) energy harvesting performance of BCZT interconnected porous composite. Reproduced with permission. Copyright 2018, Royal Society of Chemistry. (b) output voltage and power of 3D interconnected

Sm-PMN-PT skeleton-based composite. Reproduced with permission.¹⁴⁹ Copyright 2018, Elsevier. (c) energy harvesting performance of 3D-printed PNN-PZT ceramic-polymer grid-composite. Reproduced with permission.¹⁰⁶ Copyright 2020, Elsevier. (d) energy harvesting performance of 2-2 type PZN-PZT/PDMS composites. Reproduced with permission.¹³⁸ Copyright 2020, Royal Society of Chemistry. (e) output voltage and current of gradient porous PZT composite. Reproduced with permission.¹⁵⁵ Copyright 2020, Royal Society of Chemistry. (f) energy harvesting performance of flexible pillar-base structured BCZT/PDMS composites.¹⁵⁶ Copyright 2021, Elsevier.

6.1.2 Pyroelectric energy harvesting

Ferroelectric materials are able to convert temperature fluctuations into electric energy via the pyroelectric effect. The capability for generating electric power from thermal fluctuations can be assessed by the pyroelectric energy harvesting figure of merit via eqn (2). It can be deduced from above equation that more energy can be harvested by ferroelectric materials with high pyroelectric coefficient, low dielectric constant and low volume specific heat capacity. It has been demonstrated that the introduction of pores can decrease the dielectric constant and the volume specific heat capacity of ferroelectric materials. Thus, porous ferroelectric materials are promising candidates for pyroelectric energy harvesting.

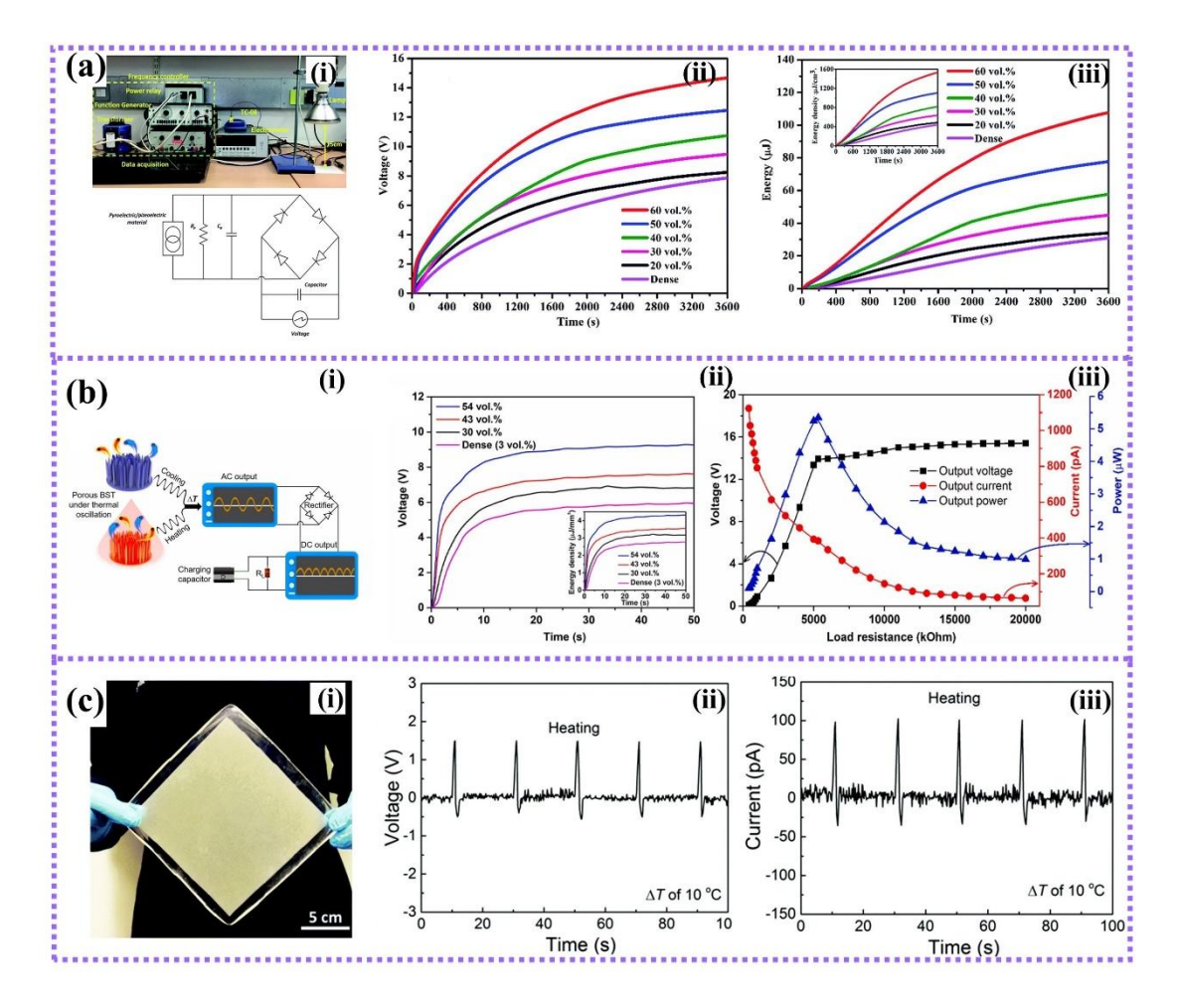


Fig. 15 Pyroelectric energy harvesting applications. (a) charging voltage and energy of parallel-connected porous PZT ceramics. Reproduced with permission.¹⁸ Copyright 2017, Royal Society of Chemistry. (b) charging voltage and power of porous BST ceramics. Reproduced with permission.¹⁵⁷ Copyright 2021, Elsevier. (c) the pyroelectric output voltage and current of the 3-D composites under a temperature fluctuation of 10 °C. Reproduced with permission.⁹⁷ Copyright 2018, Royal Society of Chemistry.

Zhang *et al.* fabricated porous PZT ceramics with aligned pore structure by freeze casting and evaluated the pyroelectric energy harvesting performance. It can be seen from Fig. 15a that the maximum voltage of 15.2 V can be obtained with a 60 vol% parallel-connected porous PZT ceramic. The maximum energy density to thermal

oscillations was 1653 mJ/cm, which was 374% higher than that of the dense PZT ceramic.¹¹⁸ Subsequently, Bao et al. presented a hierarchically structured porous pyroelectric barium strontium titanate (BST) ceramic and evaluated the pyroelectric energy harvesting performance. At the highest porosity level of 54 vol%, the output power generated reached the maximum value of 5.4 µW using an optimal external load resistance of 5.3 M Ω , as shown in Fig. 15b. Porous ferroelectric polymers have also been used for pyroelectric energy harvesting applications.¹⁵⁸ A porous Er³ modified poly(vinylidene fluoride) (PVDF) film was developed for converting thermal energies into electrical energy.¹⁵⁹ In addition, a 3-3 type of piezoelectric composite based on three-dimensional interconnected PZT skeleton was developed to harvest thermal energy. As shown in Fig. 15c, the pyroelectric output voltage of 1.6 V was obtained under the heating-cooling cycles from 25 °C to 35 °C. However, the studies of using porous ferroelectric materials for the applications of pyroelectric energy harvesting are still limited and there is a challenge is achieving high frequency thermal oscillations in contrast to mechanical vibrations.

6.2 Sensors

Ferroelectric materials can also work as sensors to detect force, strain and acceleration. One advantage of piezoelectric sensors is that they do not need external power supply compared with other types of sensors, such those that rely on piezoresistive and piezo-capacitive effects. In recent years, porous ceramic-based ferroelectric composites have attracted much interest in the field of sensing applications due to high piezoelectric voltage coefficient and good flexibility. Zhang *et al.* proved

the potential of using 3D interconnected porous piezoelectric composite for selfpowered mechanical sensing system, as shown in Fig. 16a. Once the sensor is pressed, it generates a signal and transmits it to the signal processing circuit, where the receiving circuit will control the relay in external circuit to realize the function of the wireless switch. 160 Xie et al. fabricated porous PZT-PDMS composites via freeze casting and designed piezoelectric sensors working in different modes based on the proposed architectures, as seen in Fig. 16b. It was demonstrated that the sensor could operate in a d_{31} mode to measure the strain of the vehicle wheel. In addition, the sensitivity was approximately 445 mV/N for a singular shear structure and 694 mV/N for the longitudinal sensing mode. 161 Moreover, Rana et al. demonstrated a self-powered wireless sensing system based on a porous polyvinylidene fluoride (PVDF), which is anticipated for developing autonomously-operated sensor networks, as shown in Fig. 16c. Interestingly, Cui et al. designed a three-dimensional structural node unit assembled from parameterized projection patterns and manufactured porous piezoelectric composite with complex micro-architectures for sensing applications. It was shown that the piezoelectric sensor can detect forces from different directions and provide high sensitivities due to the unique structural design, which provided a new strategy for the design of porous piezoelectric sensors. Moreover, porous ferroelectric materials can be used for SONAR applications.⁹³, 162 For example, Marselli et al used porous PZT ceramics for hydrophone applications. It was observed that the hydrophone is characterized by a high sensitivity of approximately 193 dB, indicating that porous piezoelectric ceramics can be successfully used in hydrophones. Since the pores have

potential to dampen electro-mechanical resonances, porous ferroelectric ceramic also provide a route to create broadband hydrophones for wide frequency of operation.

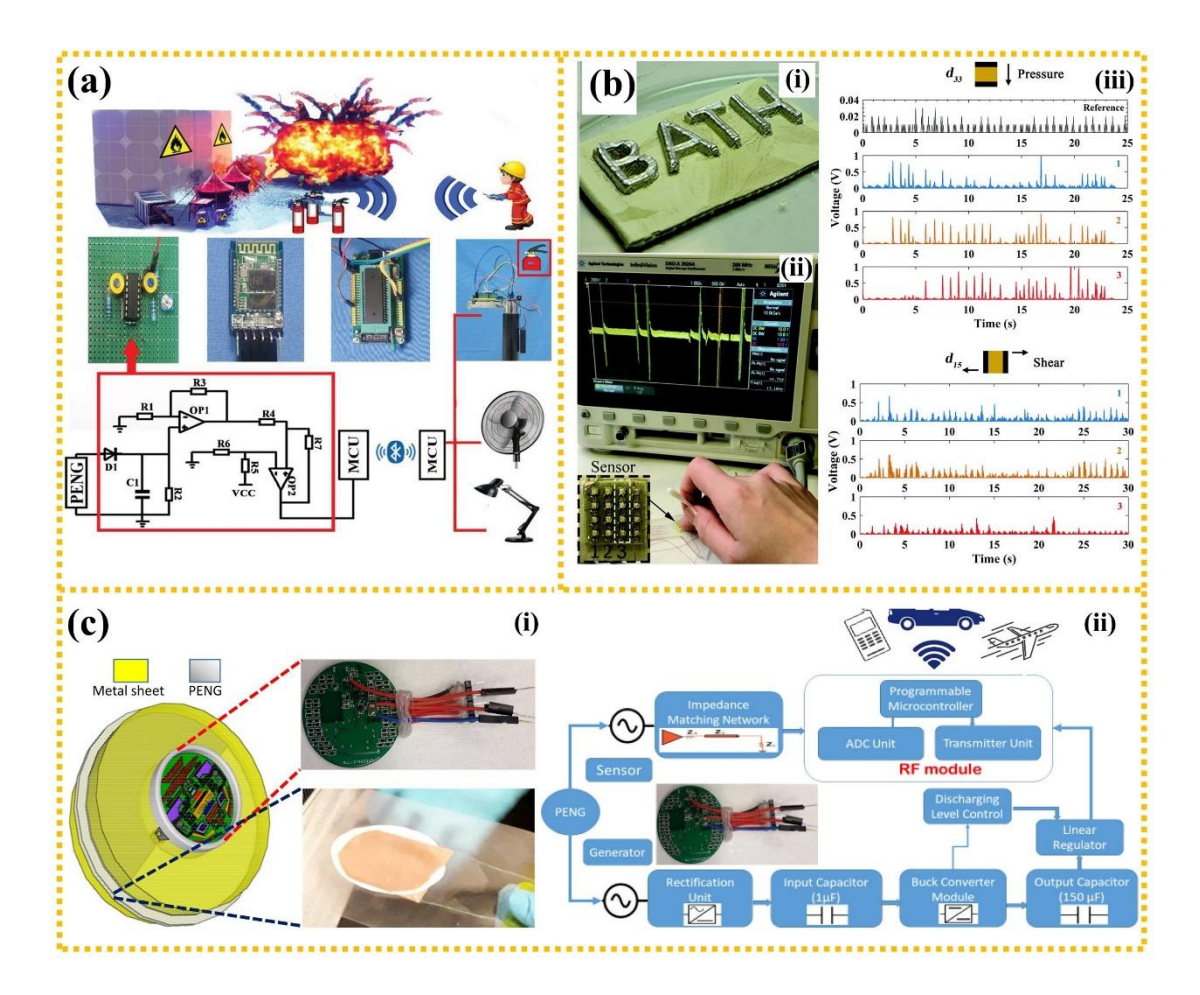


Fig. 16 Sensor applications. (a) self-powered mechanosensation system based on 3D interconnected porous piezoelectric composite. Reproduced with permission. Copyright 2019, Wiley-VCH. (b) porous PZT composite sensor's response to light finger tapping and shearing. Reproduced with permission. Copyright 2018, Royal Society of Chemistry. (c) porous PZT composite sensor's response to light finger tapping and shearing. Reproduced with permission. Copyright 2020, American Chemistry Society.

6.3 Biomedical applications

Bone tissue is demonstrated to be piezoelectric material with a low piezoelectric

coefficient, which would respond to mechanical stress, leading to the change of polarization. Many groups have made efforts to employ piezoelectric materials for potential bone substitute materials for improving the implant performance. Moreover, it has been proven that porous materials are greatly favorable to the healing process in the bone replacement due to the interconnected pores to provide a good environment for bone ingrowth. Therefore, porous ferroelectric materials are good candidates for bone tissue engineering. Porous barium titanate/hydroxyapatite composites with high piezoelectric coefficients fabricated by freeze casting were studied for bone tissue engineering. It was found that the porous piezoelectric composites exhibited no cytotoxic effects on the L929 cells, and has good biocompatibility.^{8 6} Similarly, Polley et al. manufactured porous barium titanate and hydroxyapatite composite scaffolds via a three-dimensional printing process. The printed scaffold exhibited a piezoelectric charge constant of $d_{33} \sim 3$ pC/N, LIVE/DEAD screening analysis revealed the high cytocompatibility of the porous scaffold. This study provided a promising approach to fabricate porous piezoelectric scaffold with an interconnected porous network for bone tissue engineering.²⁵ Therefore, more research should be conducted to investigate the effect of microstructure and porosity of porous ferroelectric materials for bone tissue engineering.

6.4 Catalysis applications

Piezoelectric and pyroelectric catalysis have received increasing interest for the treatment of dye wastewater, water splitting and organic catalysis due to the high efficiency and self-powered property, since ferroelectric materials can directly convert

mechanical into chemical energy by an external mechanical-force-induced piezoelectric potential or convert heat into chemical energy via temperaturefluctuation-induced polarization variations. Nanostructured ferroelectric materials are commonly used for catalysis owing to high specific surface areas. Moreover, porous nanostructures are drawing interest for catalysis applications. For example, they? exhibited excellent catalytic activity for the synthesis of 5-substituted-1H-tetrazoles using different nitriles and sodium azide. 167 h addition, Su et al. successfully synthetized BaTiO moparticles with a designed porous structure. The porous nanoparticles possessed a high overall water-splitting activity, with H production rates of 159 mmolg@1h@1, which is almost 130 times higher than that of the pristine BaTio nanoparticles. However, nanostructured and particulate-based catalysts cannot enter into the aqueous pollutant, which limits its ability to be recycled and reused. In recent years, porous ferroelectric composites consisting of ferroelectric nanoparticles and polymers have exhibited great potential for catalysis applications because of the advantages of recyclability and reuse. Qian et al. fabricated BTO-PDMS composites as porous composite catalyst to successfully realize piezoelectric catalysis. It was shown that the porous foam can degrade Rhodamine B dye solution by ~94%, showing outstanding cycle stability for repeatable decomposition testing of 12 cycles, see Fig. 17a.169 Subsequently, Xu et al. realized an enhanced photo-piezo-catalytic coupling effect for dye wastewater degradation through a porous foam made of barium strontium titanate nanoparticles and PDMS. It can be seen from Fig. 17b that the degradation efficiency reached a high level of 97.8%. An enhanced performance of 275% was

observed when compared to individual photocatalysis or low-frequency piezoelectric catalysis, since the photo-piezo-catalytic coupling effect increased the generation of electron-hole pairs.¹⁷⁰ Shi *et al.* a developed a porous piezocatalytic PVDF-BaTiQ foam through a template-molding process, and it can efficiently degrade the organic pollutants in water.¹⁷¹ Moreover, a porous polymeric composite film of rGO-F/PVDF-HFP was prepared using a modified phase-inversion process, and it was used for dye degradation and hydrogen evolution, which exhibited superior catalytic properties (Fig. 17c).¹⁷² The application of porous ferroelectric materials for pyroelectric catalysis was also explored. Min *et al.* proposed a porous pyroelectric membrane consisting of the porous PVDF film embedded with pyroelectric barium titanate nanoparticles, as shown in Fig. 17d, a strong pyro-catalytic effect with ~75% degradation efficiency for the Rhodamine B dye was achieved.¹⁷³ These studies provided a potential application for porous ferroelectric materials in the field of degrading organic pollutants in water.

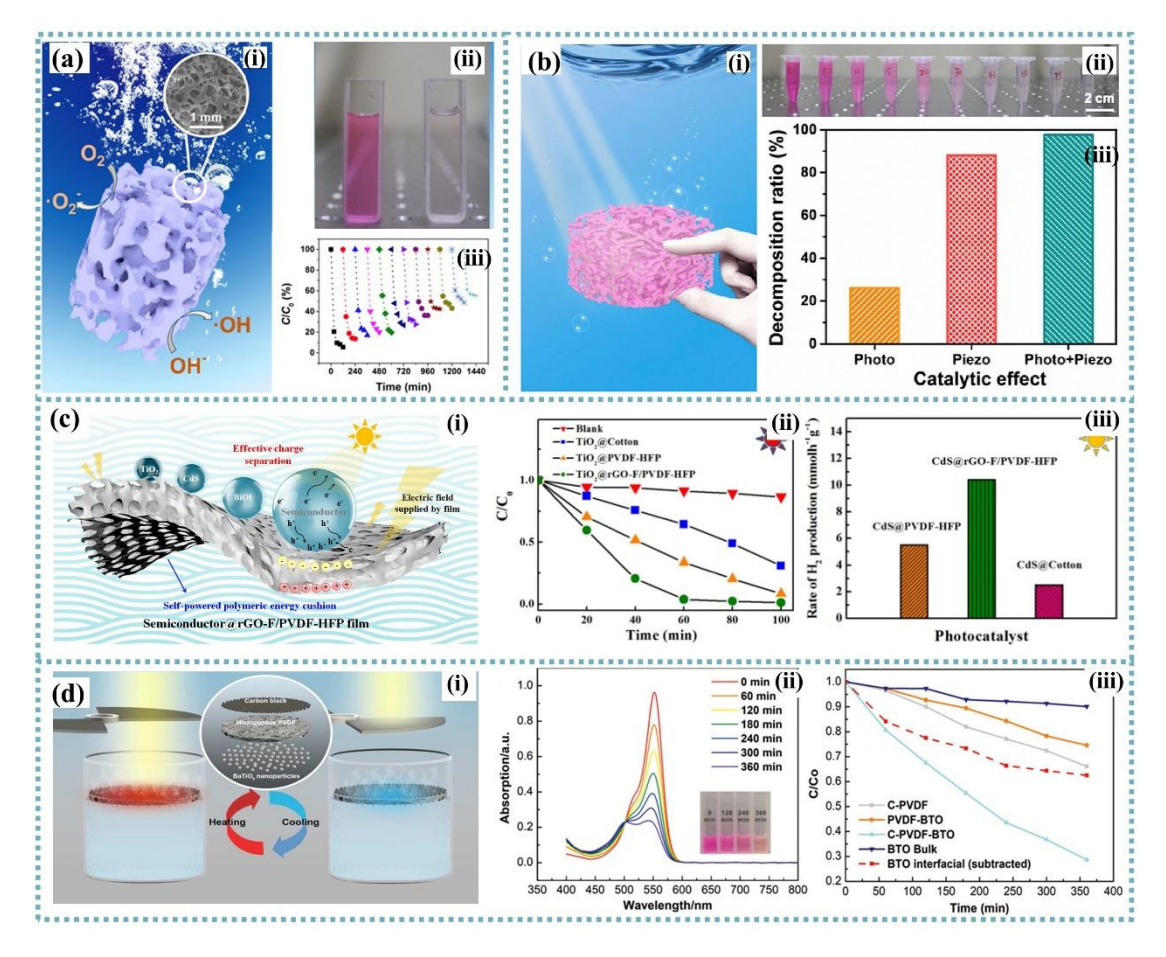


Fig. 17 Catalysis applications. (a) Piezo-catalytic activity of the BTO-PDMS composite porous foam catalyst. Reproduced with permission. Copyright 2019, American Chemistry Society. (b) BST-PDMS porous foam for the photo-piezo-catalysis. Reproduced with permission. Copyright 2020, Elsevier. (c) porous rGO-F/PVDF-HFP film for the piezoelectric catalysis. Reproduced with permission. Copyright 2018, Elsevier. (d) pyroelectric catalysis applications of porous BT-PVDF composite. Reproduced with permission. Copyright 2018, American Chemistry Society.

6.5 Energy storage applications

Ferroelectric materials can also be applied in energy storage applications due to their high power density, fast charge–discharge capability, and long lifetime. 174,175 With

regard to porous ferroelectric ceramics, there are limited reports on their application as energy storage capacitors, although the introduction of pores can reduce their breakdown strength. As shown in Fig. 18a, Luo et al. designed a 3D-BaTiO porous network as a polymer composite, where a high relative permittivity of $\varepsilon_r \sim 34.5$ was achieved with only 16 vol% 3D-BaTiO network, and the discharged energy density was over 16 times larger than the pure epoxy resin.⁵² Subsequently, Guo *et al.* produced highly aligned lamellar barium titanate (BaTiO)architectures via freeze casting, and an epoxy resin was infiltrated within the pores to form a BaTiQ /epoxy composite. An extremely high permittivity of $\varepsilon_r \sim 1408$ at 1 kHz was achieved.⁵⁴ In addition, a high discharge energy density of 19.6×10 Jcm was achieved at low electric field, which was 6.5 times higher than those of composites based on randomly distributed BaTiQ particles in an epoxy matrix, as shown in Fig. 18b. For porous ceramic-based ferroelectric composites, epoxy was chosen as the polymer matrix due to its low viscosity and good liquidity, but the permittivity of epoxy is relatively low. Therefore, Zhang et al. employed a mixture of PVDF and epoxy as the matrix to fabricate porous ceramic-based ferroelectric composite and it was demonstrated that the energy storage density was enhanced by more than three times in comparison with the PVDF-epoxy polymer matrix.⁴⁰ Although porous ceramic-based ferroelectric composites exhibit potential for energy storage capacitors due to the high relative permittivity, their lower breakdown strength compared with ferroelectric polymer can restrict their applications. In the future, the selection of polymer matrix should be optimized, and PVDF and its copolymers can be considered.

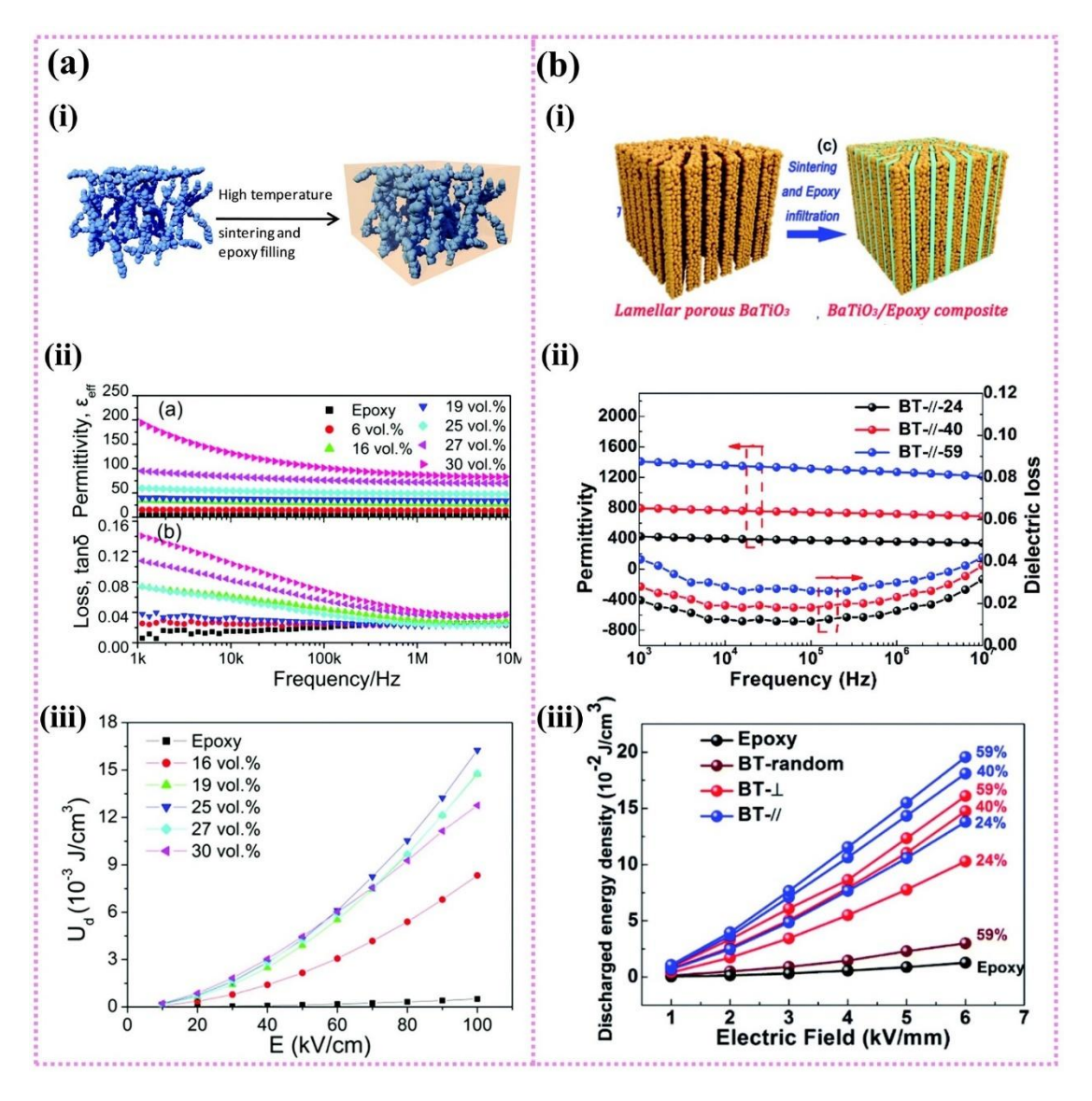


Fig. 18 Energy storage applications. (a) Permittivity and discharged energy density of 3D-BaTiQ network in polymer composites. Reproduced with permission.^{5 2} Copyright 2017, Royal Society of Chemistry. (b) Permittivity and discharged energy density of highly aligned BaTiQ /epoxy composites. Reproduced with permission.^{5 4} Copyright 2020, Royal Society of Chemistry.

7. Conclusions and prospective

Porous ferroelectric materials have attracted significant attention for their applications in energy and sensing technologies fields recent decades due to their high sensitivity to mechanical and thermal loads, and energy harvesting figures of merit. We have reviewed in detail recent progress in porous ferroelectric materials, with a focus on the classification, fabrication techniques, ferroelectric properties, analytical modelling, and applications. Overall, significant effort has been made to the progress of porous ferroelectric materials, but challenges remain to overcome, where the current status and future research directions of porous ferroelectric materials are presented in Fig. 19.

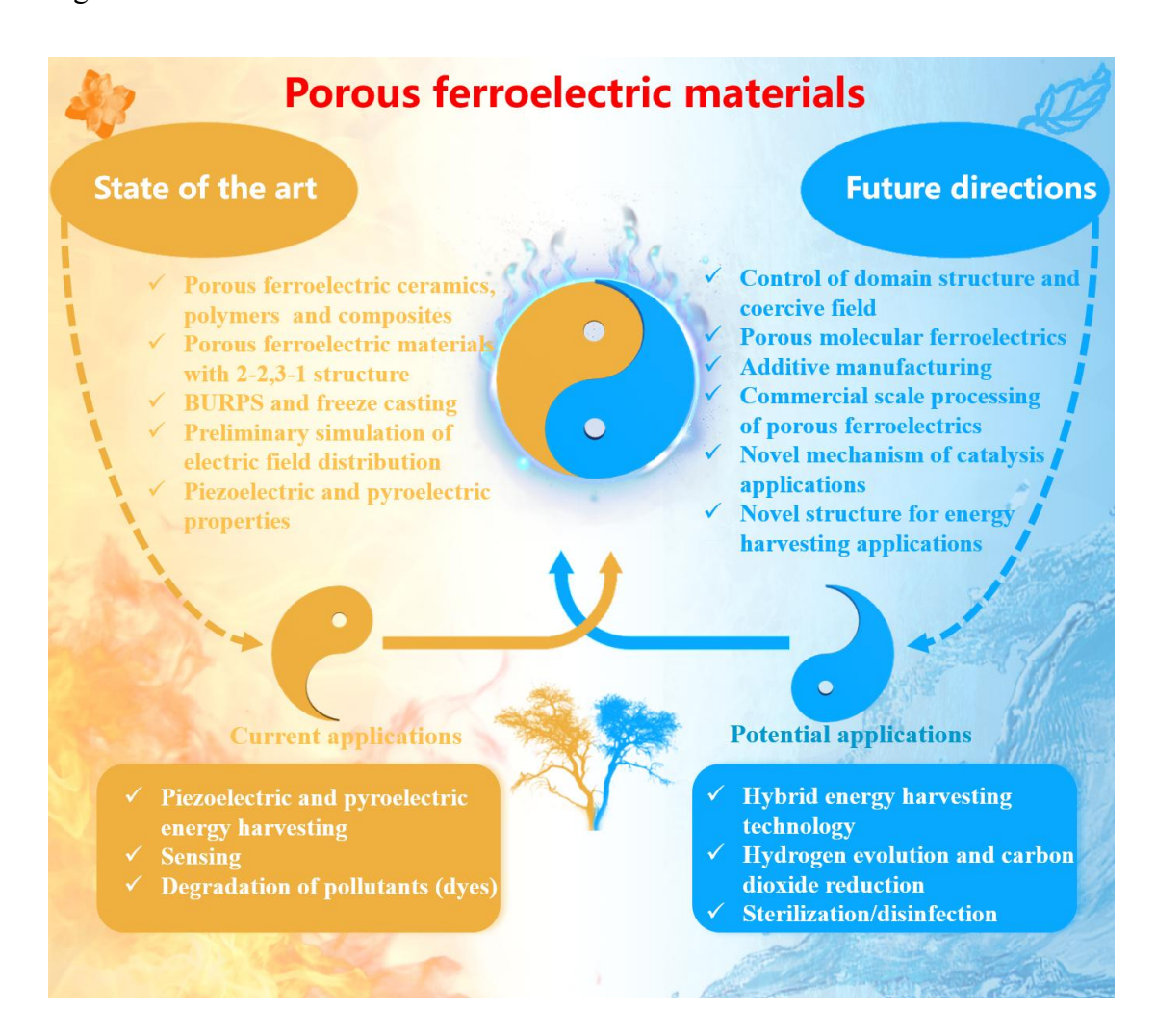


Fig. 19 Summary of current status and future research directions of porous ferroelectric materials.

- (1) Porous ferroelectric ceramics are the most widely studied porous ferroelectric materials, generally they include 3-0, 3-1, 3-3 and 2-2 type structures according to the pore connectivity. Among them, the 3-1 and 2-2 type porous ferroelectric ceramics have improved piezoelectric and pyroelectric energy harvesting performance due to the orientation of ferroelectric phase. However, the brittle nature and low fracture toughness of ceramics restricts their applications. While porous ferroelectric polymers, which often refer to porous PVDF and its copolymers, possess good flexibility and biocompatibility, their piezoelectric and pyroelectric coefficients are relatively low. Porous ceramic-based ferroelectric composites, which combine the excellent ferroelectric properties of ceramics and the flexibility of polymers, exhibit significant potential for sensing and energy harvesting applications. In addition, porous ferroelectric thin films and nanomaterials are also of interest, but the number of studies to date is relatively small and further work would be of interest.
- (2) The fabrication techniques of porous ferroelectric materials include the burnt-out polymer spheres method, replica template, gel casting freezing casting and additive manufacturing; where each method has advantages and disadvantages. Freeze casting is a promising method for fabricating porous ferroelectric materials since the porosity, pore morphology, pore size and pore orientation can be well controlled by this method. 3-1 or 3-3 type of porous ferroelectric ceramics with a highly

aligned pore structure can be obtained via freeze casting, which exhibit improved properties than those fabricated by other methods. In addition, additive manufacturing is attractive since it shows unique advantages for producing porous ferroelectric materials of complex geometry and pore structure. Existing fabrication methods can be combined with additional manufacture, for example the combination of freeze casting and additive manufacturing.

- (3) The properties of porous ferroelectric materials have been systematically summarized, including the microstructure, dielectric properties, piezoelectric properties, pyroelectric properties, and mechanical strength. The properties of porous ferroelectric materials are greatly influenced by their microstructure. Porous ferroelectric materials with aligned pore structure show higher dielectric constant, higher piezoelectric coefficients, better mechanical strength, and higher piezoelectric and pyroelectric figures of merit compared to their counterparts with randomly distributed porosity. Future studies should be focused on the optimize the structure of porous materials to enhance their energy harvesting performance. For example, there is scope for further effort in understanding the role of porosity of domain structure, domain switching kinetics and key ferroelectric properties.
- (4) Finite element modelling methods of porous ferroelectric materials have been reviewed to investigate the effect of pore shape and pore orientation to the electric distribution, polarization, and piezoelectric properties. It has been demonstrated that the electric field distribution in porous ceramics with spherical pores and orientated pores leads to higher polarization and piezoelectric coefficients. Moreover, porous

ceramic-based ferroelectric composites with 3-3 or 2-2 structure show a higher piezoelectric voltage than that of particle-based 0-3 type of composite. More attention should be paid to the modelling of pore structure and pore geometry for the polarization and piezoelectric properties.

- (5) Porous ferroelectric materials can be used for energy harvesting, sensing, catalysis, and bone tissue engineering applications. A promising application is piezoelectric energy harvesting, where numerous studies have been conducted. The 3-3 and 2-2 type porous ceramic-based ferroelectric composites exhibit potential for piezoelectric energy harvesting. The applications of pyroelectric energy harvesting are less clear due to the slow nature of thermal fluctuations, but there is potential for improved thermal sensors. Hybrid energy harvesting that combines piezoelectric, pyroelectric and photoelectric effects are more promising for future development. In addition, novel applications of using porous ferroelectric composites for hydrogen evolution and reduction of carbon dioxide will attract increasing interest due to the advantages of recyclability and high efficiency in the near future.
- (6) The understanding developed on using pore structure to improve the properties and performance of ferroelectric materials can also be applied to non-ferroelectric polar materials that exhibit piezoelectric and pyroelectric effects. For example, the use of porosity to control polarization and manage stress in thin-films of polar semi-conductors such as GaN.¹⁷⁶

Overall, this review has summarized the significant progress in porous ferroelectric materials for energy technologies in the last few years, which is expected

to serve as a useful guideline for future researches in this field. We are expecting to see more and more inspirational developments in porous ferroelectric materials in the future.

Acknowledgements

The authors acknowledge the National Natural Science Foundation of China (No. U19A2087), Key Research and Development Project of Hunan Province (No. 2020WK2004), Overseas Talent Introduction Project of China, Hundred Youth Talents Program of Hunan and State Key Laboratory of Powder Metallurgy, Central South University, Changsha, China, The Leverhulme Trust (RGP-2018-290).

Declaration of Competing Interest

The authors declare that they have no known competing financial interests or personal relationships that could have appeared to influence the work reported in this paper.

References

- 1. C. R. Bowen, H. A. Kim, P. M. Weaver and S. Dunn, *Energy Environ. Sci.*, 2014, 7, 25-44.
- 2. C. R. Bowen, J. Taylor, E. LeBoulbar, D. Zabek, A. Chauhan and R. Vaish, *Energy Environ. Sci.*, 2014, 7, 3836-3856.
- 3. X. Chen, Z. Ren, M. Han, J. Wan and H. Zhang, *Nano Energy*, 2020, **75**, 104980.
- 4. Q. Xu, J. Wen and Y. Qin, *Nano Energy*, 2021, **86**, 106080.
- 5. S. Korkmaz and İ. A. Kariper, *Nano Energy*, 2021, **84**, 105888.
- Y. Hui, J. S. Gomez-Diaz, Z. Qian, A. Alu and M. Rinaldi, *Nat Commun*, 2016,
 7, 11249.
- 7. X. Gao, X. Xin, J. Wu, Z. Chu and S. Dong, *Appl. Phys. Lett.*, 2018, **112**, 152902.
- 8. S. Li, Z. Zhao, J. Zhao, Z. Zhang, X. Li and J. Zhang, ACS Appl. Nano Mater., 2020, 3, 1063-1079.
- 9. N. Sezer and M. Koç, *Nano Energy*, 2021, **80**, 105567.
- 10. Z. L. W. J. Song, Science, 2006, 312, 242.
- 11. Y. Zhang, P. T. T. Phuong, E. Roake, H. Khanbareh, Y. Wang, S. Dunn and C. Bowen, *Joule*, 2020, 4, 301-309.
- 12. J. F. Scott, Science, 2007, 315, 954.
- 13. T. Rödig, A. Schönecker and G. Gerlach, *J. Am. Ceram. Soc.*, 2010, 93, 901-912.
- 14. R. V. Mangalam, J. C. Agar, A. R. Damodaran, J. Karthik and L. W. Martin, *ACS Appl Mater Interfaces*, 2013, **5**, 13235-13241.

- 15. C. R. Bowen, J. Taylor, E. Le Boulbar, D. Zabek and V. Y. Topolov, *Mater. Lett.*, 2015, **138**, 243-246.
- 16. P. Talemi, M. Delaigue, P. Murphy and M. Fabretto, *ACS Appl Mater Interfaces*, 2015, **7**, 8465-8471.
- 17. N. S. Sowmya, P. Varade, N. Venkataramani and A. R. Kulkarni, *J. Eur. Ceram.*Soc., 2020, 40, 5384-5391.
- 18. C. Zhou, J. Zhang, W. Yao, D. Liu and W. Su, Scr. Mater., 2019, 162, 86-89.
- 19. A. Yang, C.-A. Wang, R. Guo, Y. Huang and C.-W. Nan, *Ceram. Int.*, 2010, **36**, 549-554.
- T. Zeng, X. L. Dong, H. Chen and Y. L. Wang, *Mater. Sci. Eng. B*, 2006, 131, 181-185.
- W. Liu, J. Xu, R. Lv, Y. Wang, H. Xu and J. Yang, Ceram. Int., 2014, 40, 2005-2010.
- 22. T. Zeng, X. Dong, C. Mao, S. Chen and H. Chen, *Mater. Sci. Eng. B*, 2006, **135**, 50-54.
- 23. W. Wang, L. D. Wang, W. L. Li, D. Xu, Y. F. Hou and W. D. Fei, *J. Alloy. Compd.*, 2015, **624**, 284-289.
- 24. A. Yang, C. A. Wang, R. Guo, Y. Huang and C.-W. Nan, *J. Am. Ceram. Soc.*, 2010, **93**, 1427.
- 25. C. Polley, T. Distler, R. Detsch, H. Lund, A. Springer, A. R. Boccaccini and H. Seitz, *Materials (Basel)*, 2020, **13**, 1773.
- 26. S. Abhinay, P. Dixit and R. Mazumder, Ferroelectrics, 2020, 557, 18-27.

- J. Han, C. Hong, X. Zhang, J. Du and W. Zhang, J. Eur. Ceram. Soc., 2010, 30, 53-60.
- 28. C. Galassi, J. Eur. Ceram. Soc., 2006, 26, 2951-2958.
- 29. E. Mercadelli and C. Galassi, *IEEE Trans Ultrason Ferroelectr Freq Control*, 2021, **68**, 217-228.
- Y. Chen, N. Wang, O. Ola, Y. Xia and Y. Zhu, *Mater. Sci. Eng. R Rep.*, 2021,
 143, 100589.
- 31. W. Wang, M. Xu, X. Xu, W. Zhou and Z. Shao, *Angew Chem Int Ed Engl*, 2020, **59**, 136-152.
- 32. M. Zhang, H. Sun, X. Liu, H. Sui and S. Xiao, *Mater. Res. Bull.*, 2020, **127**, 110862.
- 33. W. Liu, L. Du, Y. Wang, J. Yang and H. Xu, Ceram. Int., 2013, 39, 8781-8787.
- 34. S. H. Lee, S. H. Jun, H. E. Kim and Y. H. Koh, *J. Am. Ceram. Soc.*, 2007, **90**, 2807-2813.
- 35. Q. Wang, Q. Chen, J. Zhu, C. Huang, B. W. Darvell and Z. Chen, *Mater. Chem. Phys.*, 2008, **109**, 488-491.
- 36. W. Liu, D. Yang, X. Wei, S. Guo, N. Wang, Z. Tang, Y. Lu, S. Shen, L. Shi, X. Li and Z. Guo, *J Biomater Appl*, 2020, **35**, 544-552.
- 37. W. Liu and X. Ren, *Phys Rev Lett*, 2009, **103**, 257602.
- 38. X. Gao, M. Zheng, X. Yan, J. Fu, M. Zhu and Y. Hou, *J. Mater. Chem. C*, 2019, 7, 961-967.
- 39. R. E. Newnham, D. P. Skinner and L. E. Cross, *Mater. Res. Bull.*, 1978, **5**, 525.

- Z. Zhang, S. Luo, S. Yu, Z. Guan, R. Sun and C. P. Wong, *Mater. Des.*, 2018,
 142, 106-113.
- 41. A. Safari and E. K. Akdogan, *Ferroelectrics*, 2006, **331**, 153-179.
- C. R. Bowen, A. Perry, A. C. F. Lewis and H. Kara, *J. Eur. Ceram. Soc.*, 2004,
 24, 541-545.
- 43. C.R. Bowen and H. Kara, *Mater. Chem. Phys.*, 2002, **75**, 45.
- 44. R. Guo, C. A. Wang and A. Yang, *J. Eur. Ceram. Soc.*, 2011, **31**, 605-609.
- 45. Y. Zhang, J. Roscow, R. Lewis, H. Khanbareh, V. Y. Topolov, M. Xie and C. R. Bowen, *Acta Mater.*, 2018, **154**, 100-112.
- 46. X. Gao, J. Yang, J. Wu, X. Xin, Z. Li, X. Yuan, X. Shen and S. Dong, *Adv. Mater. Technol.*, 2019, **5**, 1900716.
- 47. M. T. Chorsi, E. J. Curry, H. T. Chorsi, R. Das, J. Baroody, P. K. Purohit, H. Ilies and T. D. Nguyen, *Adv Mater*, 2019, **31**, e1802084.
- 48. Q. Li and Q. Wang, *Macromol. Chem. Phys.*, 2016, **217**, 1228-1244.
- 49. C. Wan and C. R. Bowen, *J. Mater. Chem. A*, 2017, **5**, 3091-3128.
- 50. D. Chen, K. Chen, K. Brown, A. Hang and J. X. J. Zhang, *Appl. Phys. Lett.*, 2017, **110**, 153902.
- 51. D. Chen and J. X. J. Zhang, *Appl. Phys. Lett.*, 2015, **106**, 193901.
- 52. S. Luo, Y. Shen, S. Yu, Y. Wan, W. H. Liao, R. Sun and C. P. Wong, *Energy Environ. Sci.*, 2017, **10**, 137-144.
- 53. D. S. Kim, C. Baek, H. J. Ma and D. K. Kim, Ceram. Int., 2016, 42, 7141-7147.
- 54. R. Guo, J. I. Roscow, C. R. Bowen, H. Luo, Y. Huang, Y. Ma, K. Zhou and D.

- Zhang, J. Mater. Chem. A, 2020, 8, 3135-3144.
- 55. A. Matavž, A. Bradeško, T. Rojac, B. Malič and V. Bobnar, *Appl. Mater. Today*, 2019, **16**, 83-89.
- V. Stancu, M. Lisca, I. Boerasu, L. Pintilie and M. Kosec, *Thin Solid Films*,
 2007, 515, 6557-6561.
- 57. V. A Reddy, N. P. Pathak and R. Nath, *Curr. Appl. Phys.*, 2012, **12**, 451-455.
- 58. Z. Cao, A. Ding, X. He, W. Cheng and P. Qiu, *J. Cryst. Growth*, 2005, **273**, 489-493.
- 59. M. Aleksandrova, *Microelectron. Eng.*, 2020, **233**, 111434.
- M. J. Zhou, T. N. Yang, J. J. Wang, Z. H. Ren, L. Q. Chen and C. W. Nan, *Acta Mater.*, 2020, 187, 146-152.
- 61. F. F. Abdullah, A. Nemati and R. Bagheri, *Mater. Lett.*, 2015, **151**, 85-88.
- 62. E. W. Yap, J. Glaum, J. Oddershede and J. E. Daniels, *Scr. Mater.*, 2018, **145**, 122-125.
- 63. L. Du, X. Du, L. Zhang, Q. An, W. Ma, H. Ran and H. Du, *J. Eur. Ceram. Soc.*, 2018, **38**, 2767-2773.
- 64. H. T. Naeem, *Mater. Today: Proceedings*, 2020, **20**, 531-534.
- 65. T. Zeng, X. Dong, S. Chen and H. Yang, *Ceram. Int.*, 2006, **33**, 395-399.
- 66. N. H. Khansur, J. Biggemann, M. Stumpf, K. Riess, T. Fey and K. G. Webber, *Adv. Eng. Mater.*, 2020, **22**, 2000389.
- 67. F. Levassort, J. Holc, E. Ringgaard, T. Bove, M. Kosec and M. Lethiecq, *J. Electroceram.*, 2007, **19**, 127-139.

- 68. J. Tan and Z. Li, Ceram. Int., 2015, 41, S414-S420.
- 69. R. Stanculescu, C. E. Ciomaga, L. Padurariu, P. Galizia, N. Horchidan, C. Capiani, C. Galassi and L. Mitoseriu, *J. Alloy. Compd.*, 2015, **643**, 79-87.
- 70. J.-H. Eom, Y.-W. Kim and S. Raju, *J. Asian. Ceram. Soc.*, 2018, **1**, 220-242.
- 71. T. Zeng, X. Dong, C. Mao, Z. Zhou and H. Yang, *J. Eur. Ceram. Soc.*, 2007, **27**, 2025-2029.
- 72. H. Zhang, J. Li and B. Zhang, *Acta Mater.*, 2007, **55**, 171-181.
- 73. D. Piazza, C. Capiani and C. Galassi, *J. Eur. Ceram. Soc.*, 2005, **25**, 3075-3078.
- 74. B. Praveenkumar, H. H. Kumar and D. K. Kharat, *J. Mater. Sci.-Mater. Electron.*, 2006, 17, 515-518.
- 75. J. Roscow, Y. Zhang, J. Taylor and C. R. Bowen, *Eur. Phys. J. Special Topics*, 2015, **224**, 2949-2966.
- 76. O. O. Omatete, M. A.Janney and S. D.Nunn, *J. Eur. Ceram. Soc.*, 1997, **17**, 407.
- 77. A. K. Yang, C. A. Wang, R. Guo and Y. Huang, *Appl. Phys. Lett.*, 2011, **98**, 152904.
- 78. W. Liu, J. Xu, Y. Wang, H. Xu, X. Xi, J. Yang and G. Brennecka, *J. Am. Ceram. Soc.*, 2013, **96**, 1827-1831.
- 79. A. Yang, C. A. Wang, R. Guo and Y. Huang, *J. Am. Ceram. Soc.*, 2010, **93**, 1984.
- 80. D. Zhang, Y. Zhang, R. Xie and K. Zhou, *Ceram. Int.*, 2012, **38**, 6063-6066.
- 81. S. Deville, E. Saiz and A. P. Tomsia, *Biomaterials*, 2006, **27**, 5480-5489.
- 82. S. Deville, E. Saiz and A. P. Tomsia, *Acta Mater.*, 2007, **55**, 1965-1974.
- 83. S. Sadeghpour, A. Amirjani, M. Hafezi and A. Zamanian, Ceram. Int., 2014, 40,

- 16107-16114.
- 84. Y. Wu, J. Zhao, Y. Li and K. Lu, Ceram. Int., 2016, 42, 15597-15602.
- 85. G. Liu and T. W. Button, *Ceram. Int.*, 2013, **39**, 8507-8512.
- 86. Y. Zhang, L. Chen, J. Zeng, K. Zhou and D. Zhang, *Mater Sci Eng C Mater Biol Appl*, 2014, **39**, 143-149.
- 87. T. Xu and C. A. Wang, *Mater. Des.*, 2016, **91**, 242-247.
- 88. Y. Zhang, Y. Bao, D. Zhang, C. R. Bowen and L. Pilon, *J. Am. Ceram. Soc.*, 2015, **98**, 2980-2983.
- 89. S. H. Lee, S. H. Jun, H. E. Kim and Y. H. Koh, *J. Am. Ceram. Soc.*, 2008, **91**, 1912-1915.
- 90. R. Guo, C.-A. Wang and A. Yang, *J. Am. Ceram. Soc.*, 2011, **94**, 1794-1799.
- 91. S. Deville, E. Saiz, R. K. Nalla and A. P. Tomsia, *Science*, 2006, **311**, 515.
- 92. P. Dixit, S. Seth, B. Rawal, B. P. Kumar and H. S. Panda, *J. Mater. Sci.-Mater. Electron.*, 2021, **32**, 5393-5403.
- 93. H. Kara, R. Ramesh, R. Stevens and C. R. Bowen, *IEEE Trans. Ultrason.*Ferroelectr. Freq. Control, 2003, **50**, 289.
- 94. M. Kim, R. A. Franco and B.-T. Lee, *J. Eur. Ceram. Soc.*, 2011, **31**, 1541-1548.
- 95. I. Narkevica, L. Stipniece, E. Jakobsons, I. Cakstina and J. Ozolins, *J. Eur. Ceram. Soc.*, 2017, **37**, 833-840.
- C. Voigt, C. G. Aneziris, J. Hubálková and G. Franks, *J. Am. Ceram. Soc.*, 2015,
 98, 1460-1463.
- 97. G. Zhang, P. Zhao, X. Zhang, K. Han, T. Zhao, Y. Zhang, C. K. Jeong, S. Jiang,

- S. Zhang and Q. Wang, Energy Environ. Sci., 2018, 11, 2046-2056.
- 98. Y. Zhang, C. K. Jeong, T. Yang, H. Sun, L.-Q. Chen, S. Zhang, W. Chen and Q. Wang, *J. Mater. Chem. A*, 2018, **6**, 14546-14552.
- 99. E. C. Bucharsky, K. G. n. Schell, R. Oberacker and M. J. Hoffmann, *J. Am. Ceram. Soc.*, 2010, **93**, 111-114.
- 100. H. Dommati, S. S. Ray, J.-C. Wang and S.-S. Chen, *RSC Adv.*, 2019, **9**, 16869-16883.
- 101. S. L. Morissette and J. A. Lewis, *J. Am. Ceram. Soc.*, 2001, **84**, 2462.
- 102. B. A. Tuttle, J. E. Smay, J. C. III and J. A. Voigt, J. Am. Ceram. Soc., 2001, 84, 872.
- 103. J. E. Smay, J. C. III, B. A. Tuttle and J. A. Lewis, *J. Am. Ceram. Soc.*, 2004, **87**, 293.
- 104. J. E. Smay, J. Cesarano, B. A. Tuttle and J. A. Lewis, *J. Appl. Phys.*, 2002, 92, 6119-6127.
- B. Nan, S. Olhero, R. Pinho, P. M. Vilarinho, T. W. Button and J. M. F. Ferreira,
 J. Am. Ceram. Soc., 2018, 102, 3191-3203.
- 106. Z. Wang, X. Yuan, J. Yang, Y. Huan, X. Gao, Z. Li, H. Wang and S. Dong, *Nano Energy*, 2020, **73**, 104737.
- 107. C. Shuai, G. Liu, Y. Yang, F. Qi, S. Peng, W. Yang, C. He, G. Wang and G. Qian, *Nano Energy*, 2020, **74**, 104825.
- 108. K. Yako, H. Kakemoto, T. Tsurumi and S. Wada, *Mater. Sci. Eng. B*, 2005, 120, 181-185.

- 109. T. Xu, C. A. Wang and H. E. Kim, *J. Am. Ceram. Soc.*, 2015, **98**, 2700-2702.
- 110. S. Zhu, L. Cao, Z. Xiong, C. Lu and Z. Gao, *J. Eur. Ceram. Soc.*, 2018, **38**, 2251-2255.
- 111. J. Tan and Z. Li, J. Mater. Sci., 2016, **51**, 5092-5103.
- 112. W. Wang, M. Zhang, L. Xin, S. Shen and J. Zhai, *J. Alloy. Compd.*, 2019, **809**, 151712.
- 113. O. V. Malyshkina, E. V. Barabanova, N. E. Malysheva, A. Kapustkin and A. I. Ivanova, *Ferroelectrics*, 2020, **561**, 114-119.
- 114. L. Curecheriu, V. A. Lukacs, L. Padurariu, G. Stoian and C. E. Ciomaga, *Materials (Basel)*, 2020, **13**, 3324.
- 115. Y. Zhang, C. R. Bowen and S. Deville, *Soft Matter*, 2019, **15**, 825-832.
- L. Du, P. Zhang, L. Wang, B. Zheng and H. Du, *Comput. Mater. Sci.*, 2017, 131, 196-201.
- 117. Y. Zhang, J. Roscow, M. Xie and C. Bowen, *J. Eur. Ceram. Soc.*, 2018, **38**, 4203-4211.
- 118. Y. Zhang, M. Xie, J. Roscow, Y. Bao, K. Zhou, D. Zhang and C. R. Bowen, *J. Mater. Chem. A*, 2017, **5**, 6569-6580.
- H. T. Kim, J. H. Ji, B. S. Kim and J. H. Koh, Ceram. Int., 2020, 46, 25050-25057.
- 120. V. A. Lukacs, G. Caruntu, O. Condurache, C. E. Ciomaga, L. P. Curecheriu, L. Padurariu, M. Ignat, M. Airimioaei, G. Stoian, A. Rotaru and L. Mitoseriu, Ceram. Int., 2021, 47, 18105-18115.

- 121. R. N. Nandini, M. Krishna, A. V. Suresh and H. N. Narasimha Murthy, *Mater. Sci. Eng. B*, 2018, **231**, 40-56.
- 122. Y. Zhang, M. Xie, J. Roscow and C. Bowen, *Mater. Res. Bull.*, 2019, **112**, 426-431.
- V. A. Lukacs, R. Stanculescu, L. Curecheriu, C. E. Ciomaga, N. Horchidan, C.
 Cioclea and L. Mitoseriu, *Ceram. Int.*, 2020, 46, 523-530.
- 124. H. Nie, X. Dong, N. Feng, X. Chen, G. Wang, Y. Gu, H. He and Y. Liu, *Mater. Res. Bull.*, 2011, **46**, 1243-1246.
- 125. M. Chen, Y. Pu and L. Zhang, J. Alloy. Compd., 2021, 877, 160225.
- 126. B. P. Kumar, H. H. Kumar and D. K. Kharat, *Mater. Sci. Eng. B*, 2006, **127**, 130-133.
- 127. J. Schultheiß, J. I. Roscow and J. Koruza, *Phys. Rev. Mater.*, 2019, **3**, 084408.
- D. Piazza, L. Stoleriu, L. Mitoseriu, A. Stancu and C. Galassi, *J. Eur. Ceram. Soc.*, 2006, 26, 2959-2962.
- 129. J. L. Butler, J Acoust Soc Am, 2012, 132, 2158-2160.
- D. J. Shin, D. H. Lim, B. K. Koo, M. S. Kim, I. S. Kim and S. J. Jeong, *J. Alloy. Compd.*, 2020, 831, 154792.
- 131. A. N. Reznichenko, M. A. Lugovaya, E. I. Petrova, N. A. Shvetsova and A. N. Rybyanets, *Ferroelectrics*, 2019, **539**, 93-100.
- 132. J. I. Roscow, R. W. C. Lewis, J. Taylor and C. R. Bowen, *Acta Mater.*, 2017,128, 207-217.
- 133. Y.-Y. Li, L.-T. Li and B. Li, J. Alloy. Compd., 2015, **620**, 125-128.

- 134. Y. Li, L. Li and B. Li, *Materials (Basel)*, 2015, **8**, 1729-1737.
- M. Sharma, V. P. Singh, S. Singh, P. Azad, B. Ilahi and N. A. Madhar, *J. Electron. Mater.*, 2018, 47, 4882-4891.
- K. S. Srikanth, V. P. Singh and R. Vaish, *J. Eur. Ceram. Soc.*, 2017, 37, 3943-3950.
- 137. R. Ramesh, H. Kara and C. R. Bowen, Ferroelectrics, 2002, 273, 383.
- 138. Y. Hao, Y. Hou, J. Fu, X. Yu, X. Gao, M. Zheng and M. Zhu, *Nanoscale*, 2020,12, 13001-13009.
- 139. H. Zhao, P. Wu, L. Du and H. Du, Comput. Mater. Sci., 2018, 148, 216-223.
- L. Van Lich, T. Shimada, J. Wang and T. Kitamura, *Nanoscale*, 2017, 9, 15525-15533.
- 141. H. Chen, X. Hou, J. Chen, S. Chen, P. Hu, H. Wu, J. Wang and J. Zhu, Nanotechnology, 2020, **31**, 335714.
- 142. F. Gheorghiu, L. Padurariu, M. Airimioaei, L. Curecheriu, C. Ciomaga, C. Padurariu, C. Galassi and L. Mitoseriu, *J. Am. Ceram. Soc.*, 2017, **100**, 647-658.
- 143. R. Khachaturyan, S. Zhukov, J. Schultheiß, C. Galassi, C. Reimuth, J. Koruza, H. von Seggern and Y. A. Genenko, *J. Phys. D-Appl. Phys.*, 2017, **50**, 045303.
- 144. G. Martínez-Ayuso, M. I. Friswell, H. Haddad Khodaparast, J. I. Roscow and C. R. Bowen, *Acta Mater.*, 2019, **173**, 332-341.
- J. I. Roscow, Y. Zhang, M. J. Kraśny, R. W. C. Lewis, J. Taylor and C. R. Bowen,
 J. Phys. D-Appl. Phys., 2018, 51, 225301.
- 146. R. Kargupta and T. Venkatesh, *Acta Mater.*, 2006, **54**, 4063-4078.

- P. W. Bosse, K. S. Challagulla and T. A. Venkatesh, *Acta Mater.*, 2012, 60, 6464-6475.
- 148. K. S. Challagulla and T. A. Venkatesh, *Acta Mater.*, 2012, **60**, 2111-2127.
- Y. Zhang, C. K. Jeong, J. Wang, H. Sun, F. Li, G. Zhang, L.-Q. Chen, S. Zhang,W. Chen and Q. Wang, *Nano Energy*, 2018, **50**, 35-42.
- 150. Y. Mao, P. Zhao, G. McConohy, H. Yang, Y. Tong and X. Wang, *Adv. Energy Mater.*, 2014, **4**, 1301624.
- 151. M. M. Rana, A. A. Khan, G. Huang, N. Mei, R. Saritas, B. Wen, S. Zhang, P. Voss, E. Abdel-Rahman, Z. Leonenko, S. Islam and D. Ban, ACS Appl Mater Interfaces, 2020, 12, 47503-47512.
- 152. Z. Zhou, X. Du, J. Luo, L. Yao, Z. Zhang, H. Yang and Q. Zhang, *Nano Energy*, 2021, **84**, 105895.
- 153. W. Tong, Q. An, Z. Wang, Y. Li, Q. Tong, H. Li, Y. Zhang and Y. Zhang, *Adv Mater*, 2020, **32**, e2003087.
- S. Yu, Y. Zhang, Z. Yu, J. Zheng, Y. Wang and H. Zhou, *Nano Energy*, 2021, 80, 105519.
- H. Liu, X. Lin, S. Zhang, Y. Huan, S. Huang and X. Cheng, *J. Mater. Chem. A*,
 2020, 8, 19631-19640.
- 156. M. Yan, J. Zhong, S. Liu, Z. Xiao, X. Yuan, D. Zhai, K. Zhou, Z. Li, D. Zhang,C. Bowen and Y. Zhang, *Nano Energy*, 2021, 88, 106278.
- Y. Bao, B. Huang, K. Zhou, J. Roscow, E. Roake, M. Hopkins, D. Zhang, Y.
 Zhang and C. Bowen, *Ceram. Int.*, 2021, 47, 18761-18772.

- 158. A. Navid, C. S. Lynch and L. Pilon, *Smart Mater. Struct.*, 2010, **19**, 055006.
- 159. S. K. Ghosh, M. Xie, C. R. Bowen, P. R. Davies, D. J. Morgan and D. Mandal, *Sci Rep*, 2017, **7**, 16703.
- Y. Zhang, M. Wu, Q. Zhu, F. Wang, H. Su, H. Li, C. Diao, H. Zheng, Y. Wu and
 Z. L. Wang, *Adv. Funct. Mater.*, 2019, 29, 1904259.
- 161. M. Xie, Y. Zhang, M. J. Kraśny, C. R. Bowen, H. Khanbareh and N. Gathercole, *Energy Environ. Sci.*, 2018, **11**, 2919-2927.
- 162. R. Ramesh, H. Kara and C. R. Bowen, *Ultrasonics*, 2005, **43**, 173-181.
- 163. S. Marselli, V. Pavia, C. Galassi, E. Roncari, F. Craciun and G. Guidarelli, *J. Acoust. Soc. AM*, 1999, **106**, 733-738.
- J. Chen, W. Luo, S. Yu, X. Yang, Z. Wu, H. Zhang, J. Gao, Y.-W. Mai, Y. Li and
 Y. Jia, *Ceram. Int.*, 2020, 46, 9786-9793.
- X. Xu, S. Chen, Z. Wu, Y. Jia, L. Xiao and Y. Liu, *Nano Energy*, 2018, **50**, 581-588.
- J. Ma, J. Ren, Y. Jia, Z. Wu, L. Chen, N. O. Haugen, H. Huang and Y. Liu, *Nano Energy*, 2019, 62, 376-383.
- A. Sinhamahapatra, A. K Giri, P. Pal, S. K. Pahari, H. C. Bajaj and A. B. Panda,
 J. Mater. Chem., 2012, 22, 17227-17235.
- 168. R. Su, Z. Wang, L. Zhu, Y. Pan, D. Zhang, H. Wen, Z. D. Luo, L. Li, F. T. Li,
 M. Wu, L. He, P. Sharma and J. Seidel, *Angew Chem Int Ed Engl*, 2021, 60,
 16019-16026.
- 169. W. Qian, K. Zhao, D. Zhang, C. R. Bowen, Y. Wang and Y. Yang, ACS Appl

- Mater Interfaces, 2019, 11, 27862-27869.
- 170. S. Xu, W. Qian, D. Zhang, X. Zhao, X. Zhang, C. Li, C. R. Bowen and Y. Yang, *Nano Energy*, 2020, 77, 105305.
- J. Shi, W. Zeng, Z. Dai, L. Wang, Q. Wang, S. Lin, Y. Xiong, S. Yang, S. Shang,W. Chen, L. Zhao, X. Ding, X. Tao and Y. Chai, *Small Science*, 2020, 1, 2000011.
- 172. W. Tong, Y. Zhang, H. Huang, K. Xiao, S. Yu, Y. Zhou, L. Liu, H. Li, L. Liu, T. Huang, M. Li, Q. Zhang, R. Du and Q. An, *Nano Energy*, 2018, **53**, 513-523.
- M. Min, Y. Liu, C. Song, D. Zhao, X. Wang, Y. Qiao, R. Feng, W. Hao, P. Tao,W. Shang, J. Wu and T. Deng, ACS Appl Mater Interfaces, 2018, 10, 21246-21253.
- 174. Y. Hao, X. Wang, K. Bi, J. Zhang, Y. Huang, L. Wu, P. Zhao, K. Xu, M. Lei and L. Li, *Nano Energy*, 2017, **31**, 49-56.
- 175. P. Zhao, H. Wang, L. Wu, L. Chen, Z. Cai, L. Li and X. Wang, *Adv. Energy Mater.*, 2019, **9**.
- Y. Calahorra, B. Spiridon, A. Wineman, T. Busolo, P. Griffin, P. K. Szewczyk,
 T. Zhu, Q. Jing, R. Oliver and S. Kar-Narayan, *Appl. Mater. Today*, 2020, 21, 100858.